The American Journal of Pathology, Vol. 191, No. 8, August 2021

ELSEVIER

The American Journal of
PATHOLOGY
ajp.amjpathol.org

MOLECULAR PATHOGENESIS OF GENETIC AND INHERITED DISEASES

# Human *RGR* Gene and Associated Features of Age-Related Macular Degeneration in Models of Retina-Choriocapillaris Atrophy



Xuan Bao,[*†] Zhaoxia Zhang,[†‡] Yanjiang Guo,[*] Christopher Buser,[§] Harold Kochounian,[¶] Nancy Wu,[‖] Xiaohua Li,[**] Shikun He,[††] Bin Sun,[‡] Fred N. Ross-Cisneros,[¶] Alfredo A. Sadun,[¶‡‡] Lvzhen Huang,[*] Mingwei Zhao,[*] and Henry K.W. Fong[†§§¶¶]

*From the Department of Ophthalmology,* Beijing Key Laboratory for the Diagnosis and Treatment of Retinal and Choroid Diseases, Peking University People's Hospital, Beijing, China; the Departments of Ophthalmology† and Pathology†† and the Norris Cancer Center,‖ Keck School of Medicine of University of Southern California, Los Angeles, California; the Shanxi Eye Hospital,‡ Taiyuan, China; the Oak Crest Institute of Science,§ Monrovia, California; the Doheny Eye Institute,¶ Los Angeles, California; the Henan Eye Institute,** Henan Provincial People's Hospital, Henan, China; the Department of Ophthalmology,‡‡ David Geffen School of Medicine at University of California Los Angeles, Los Angeles, California; the University of Southern California Roski Eye Institute,§§ Los Angeles, California; and the Department of Molecular Microbiology and Immunology,¶¶ University of Southern California, Los Angeles, California*

Accepted for publication
May 5, 2021.

Address correspondence to Mingwei Zhao, M.D., Ph.D., Department of Ophthalmology, Beijing Key Laboratory for the Diagnosis and Treatment of Retinal and Choroid Diseases, Peking University People's Hospital, 11 Xizhimen S. St., Xi Cheng District, Beijing 100044, China; or Henry K.W. Fong, Ph.D., Department of Ophthalmology, Keck School of Medicine of University of Southern California, Mudd Memorial Research Bldg. MMR-322, 1333 San Pablo St., Los Angeles, CA 90089. E-mail: 0062011320@bjmu.edu.cn or hfong@usc.edu.

Age-related macular degeneration (AMD) is a progressive eye disease and the most common cause of blindness among the elderly. AMD is characterized by early atrophy of the choriocapillaris and retinal pigment epithelium (RPE). Although AMD is a multifactorial disease with many environmental and genetic risk factors, a hallmark of the disease is the origination of extracellular deposits, or drusen, between the RPE and Bruch membrane. Human retinal G-protein—coupled receptor (*RGR*) gene generates an exon-skipping splice variant of RGR-opsin (RGR-d; NP_001012740) that is a persistent component of small and large drusen. Herein, the findings show that abnormal RGR proteins, including RGR-d, are pathogenic in an animal retina with degeneration of the choriocapillaris, RPE, and photoreceptors. A frameshift truncating mutation resulted in severe retinal degeneration with a continuous band of basal deposits along the Bruch membrane. RGR-d produced less severe disease with choriocapillaris and RPE atrophy, including focal accumulation of abnormal RGR-d protein at the basal boundary of the RPE. Degeneration of the choriocapillaris was marked by a decrease in endothelial CD31 protein and choriocapillaris breakdown at the ultrastructural level. Fundus lesions with patchy depigmentation were characteristic of old RGR-d mice. RGR-d was mislocalized in cultured cells and caused a strong cell growth defect. These results uphold the notion of a potential hidden link between AMD and a high-frequency *RGR* allele. *(Am J Pathol 2021, 191: 1454—1473; https://doi.org/10.1016/j.ajpath.2021.05.003)*

Abnormal protein deposits at extracellular or intracellular sites are a feature of numerous neurodegenerative diseases, including Parkinson disease, Alzheimer disease, and age-related macular degeneration (AMD).[1,2] In human eyes, age-related deposits accumulate along the Bruch membrane, the innermost choroidal layer that directly underlies the retinal pigment epithelium (RPE).[3] With aging, focal extracellular deposits, referred to as small hard drusen, develop between the Bruch membrane and the RPE in most eyes.[4,5] Numerous, large, and confluent drusen, referred to as soft indistinct drusen, are a hallmark of AMD.[6,7] Despite the pathologic significance of soft confluent drusen and the association of AMD with multiple gene variants,[8,9] the

Supported in part by the Gordon and Evelyn Leslie Macular Degeneration Fund (H.K.W.F.), NIH grant R01EY08364 (H.K.W.F.), an unrestricted grant to the USC Department of Ophthalmology from Research to Prevent Blindness, New York, NY, NIH grant P30EY029220, and National Natural Science Foundation of China grant 81770943 (M.Z.).

X.B. and Z.Z. contributed equally to this work.

Disclosures: None declared.


https://doi.org/10.1016/j.ajpath.2021.05.003

mechanism of drusen formation remains elusive. To better understand drusen biogenesis and AMD pathophysiology, the lipid, carbohydrate, and protein components of drusen have been studied extensively.[10,11]

The RPE plays an important role in the formation of drusen.[12–14] Although many proteins, or protein fragments, in drusen have been identified,[11,15] the exact role of the adjacent RPE in establishment of drusen is unknown. It is believed that cellular debris from the RPE contributes to the presence of extracellular basal deposits and the growth of druse mass.[12–14,16,17] A traceable drusen-associated protein marker derived from the RPE is the exon VI–skipping splice isoform of human nonvisual opsin, retinal G-protein–coupled receptor (RGR-d).[18–20] The RGR-d isoform results from alternative splicing of *RGR* pre-mRNA with complete in-frame deletion of the exon VI sequence of the *RGR* opsin gene.[19,21] The *RGR* gene is expressed in the RPE and Müller cells.[18] In human and bovine, but not mouse, retinas, RGR opsin is also localized in cone photoreceptors and in a population of retinal ganglion cells.[22] RGR is bound to all-*trans*-retinal in the dark, and its chromophore is photoisomerized stereospecifically to 11-*cis*-retinal.[23,24] It functions in part to maintain a normal rate of 11-*cis*-retinal synthesis both in light and in darkness after irradiation.[25–28] In mice, RGR in Müller cells acts as a photoisomerase jointly with a retinol dehydrogenase to regenerate bleached cone visual pigments.[29] Light-dependent enzymatic production of 11-*cis*-retinal by RGR is increased in the presence of cellular retinaldehyde-binding protein and all-*trans*-retinal *in vitro*.[30] Humans, but not cattle or mice, synthesize both normal RGR and the extraneous, presumably nonfunctional, RGR-d. RGR-d lacks the entire transmembrane domain VI of RGR opsin. In a young individual, *RGR-d* mRNA may be as high as 17% of the copy number of normal *RGR* mRNA in the RPE.[31]

Immunologic and mass spectrometric analyses independently demonstrate the presence of RGR-d protein in human donor retina and RPE.[31] Unlike normal RGR, RGR-d does not localize to the smooth endoplasmic reticulum. Instead, the folded protein traffics to the basolateral plasma membrane of RPE cells, which is more evident in young than older donors.[32] Some amount of the RGR-d protein, or peptide fragment thereof, is released from the epithelium into the sub-RPE space and deposited into the Bruch membrane.[31,33] The extracellular RGR-d colocalizes substantially with both vitronectin and the terminal complement complex, C5b-9.[32] Like early-stage drusen, initial deposits of extracellular RGR-d accumulate at intercapillary regions in the Bruch membrane, and RGR-d is present in both hard and soft drusen.[33] Because extracellular RGR-d is closely associated with drusen deposits, it is not unexpected that the distribution pattern of RGR-d within the RPE–Bruch membrane–choriocapillaris complex is divergent between young and old individuals.[32,33]

Despite the notion that drusen formation may be driven by a futile series of RGR-d synthesis, degradation, and release,[32] currently there is no demonstration that RGR-d is actively involved in the process nor understanding of how this common, albeit abnormal, membrane protein might result in an age-related disease. The RGR-d isoform was not considered a factor in previous models of drusen formation and AMD.[34–36] Yet RGR-d is inherently problematic insofar that its synthesis may reduce the concentration of functional RGR photoisomerase, waste cellular energy and resources, and form harmful misfolded proteins under adverse conditions. The purpose of this study was to test the hypothesis that RGR-d is involved in abnormal protein accumulation and may lead to progressive retinal atrophy in a mouse model of AMD.

## Materials and Methods

### Animal Care and Use

All animals were treated, maintained, and euthanized in accordance with the Association for Research in Vision and Ophthalmology resolution on the use of animals in research and in compliance with guidelines of the US Public Health Service, as delineated in the Public Health Service Policy on Humane Care and Use of Laboratory Animals. The mice were housed in standard filter-top cages and maintained on a constant 12-hour light-dark cycle. Eight week to 2-year-old control and RGR-d mutant mice were used. At least three mice from each group were used for each experiment. For ocular histology and electron microscopy, at least eight RGR-d mice were used.

### Generation of *Rgr*$^{-/-}$ Mice

RGR$^{-/-}$ knockout mice were generated, as described previously.[25] A DNA fragment of the 129SV mouse *Rgr* gene was disrupted by insertion of a pPGK neo bpA fusion gene at a BglII site within exon II. The TK gene from the Xho PKS MCI TK vector was inserted into the plasmid at the 3′ end of the *Rgr*-neo fusion gene. The targeting vector DNA was electroporated into R1 embryonic stem cells. Embryonic stem clones were selected for homologous recombination in the presence of G418 and 2′-deoxy-2′-fluoro-β-D-arabinofuranosyl-5-iodouracil. Selected embryonic stem cells were injected into 3.5-day–old blastocysts. Mouse chimeras were obtained and were bred with C57BL/6J mice to attain germline transmission of the *Rgr* mutation.

### Generation of RGR-d Mice by Gene Editing

RGR-d mutant mice (genetic background: B6D2F1/J; Jackson Laboratory, Bar Harbor, ME) were generated by mutation of the splice site at each end of exon VI of the mouse *Rgr* gene. Alteration of the splice sites was performed by multiplex gene editing using clustered regularly interspaced short palindromic repeats (CRISPR) methods. The following pair of single guide RNAs (gRNAs)

that target the two splice sites of mouse *Rgr* exon VI was designed using the online program at http://crispr.mit.edu (last accessed June 3, 2015): T7RGRgRNAf1, 5′-GAAATTAATACGACTCACTATAGGTGGAAGAGTAGTATTCACCT GTTTTAGAGCTAGAAATAGC-3′; and T7RGRgRNAf2, 5′-GAAATTAATACGACTCACTATAGGCATCTCTCCTAAACTACAGA GTTTTAGAGCTAGAAATAGC-3′.

The pair of gRNAs (*Rgr* sequence underlined) and Cas9 mRNA (TriLink Biotechnologies, San Diego, CA) were microinjected into single-cell wild-type B6D2F1/J embryos, and mutation of either the 5′ or 3′ splice site, both splice sites, or total deletion of exon VI was anticipated.

## Analysis of Founder Mouse Genotype and Sequencing

Mouse genomic DNA was prepared by digestion of tail tissue with 0.5 mg/mL proteinase K in lysis buffer (50 mmol/L Tris-HCl, pH 8.0, 100 mmol/L EDTA, 100 mmol/L NaCl, and 1% SDS) at 55°C overnight. The samples were mixed with an equal volume of phenol/chloroform/isoamyl alcohol (25:24:1, v/v/v). After centrifugation, the upper aqueous phase was removed, and the DNA was precipitated by addition of two volumes of cold 100% ethanol. The DNA was centrifuged, rinsed with 70% ethanol, dried briefly, and dissolved in 10 mM Tris, 1 mM EDTA buffer, pH 8.0.

The mouse *Rgr* gene for each founder pup was analyzed by PCR amplification of tail genomic DNA using forward and reverse primers, respectively: mRGR-Exon6S, 5′-TTAGCATCAGCAACCTCCCC-3′; and mRGR-Exon6A, 5′-CCTCCCCGCTTGGAACTATC-3′.

PCR was performed with 5 pmol of each primer, 1 μL of genomic DNA solution, and 2.5 units of TopTaq DNA polymerase (Qiagen, Germantown, MD) for 35 cycles of 30 seconds at 94°C, 1 minute at 55°C, and 90 seconds at 72°C. The fragments were electrophoresed and visualized with GelRed (Biotium, Inc., Fremont, CA). The expected PCR product from the mouse *Rgr* gene is 924 nucleotides long (410 nucleotides from the upstream intron, 114 nucleotides of exon VI, and 400 nucleotides of the downstream intron). Each amplicon was sequenced to confirm gene editing of the splice sites or to characterize large deletions or insertions in the region of exon VI. The PCR products were purified with the QIAquick PCR purification kit (Qiagen) and sequenced using the following primer: MRGR-SEQ98(+), 5′-TCCAGACCTCTCCAAGAGCAT-3′. The 3′ end of MRGR-SEQ98(+) is 77 nucleotides from the 5′ end of exon VI.

## Analysis of Mouse *Rgr-d* mRNA

Mouse *Rgr* mRNA transcripts were analyzed by reverse transcription and PCR (Superscript III One-Step RT-PCR Platinum Taq; Invitrogen, Carlsbad, CA) and direct sequencing. Founder mice with gene modifications were bred with wild-type DBA/2J mice to provide $F_1$ offspring for mRNA analysis. Total RNA from the eyecups of positive mutant pups were isolated. The lens was removed from each eyecup, and RNA was isolated using RNAzol B/RNA-Bee (Tel-Test Inc., Friendswood, TX). Mouse *Rgr* mRNAs were reverse transcribed into cDNA using an exon VII−specific RGR primer (mRGR-Rev; 5′-GGCATGGTTTTGGCGATGAG-3′). The 3′-end of primer mRGR-Rev is located nine nucleotides from the 5′ end of exon VII. The presence of the full-length or an exon-skipping mRNA was determined by PCR analysis of the cDNA, using the mRGR-Rev primer and a forward exon III−specific RGR primer (mRGR-Fwd; 5′-CCTGGGGACGTTATCACCAC-3′). The expected size of the amplicon from intact mouse *Rgr* mRNA is 445 nucleotides, and that from mouse *Rgr-d* mRNA is 331 nucleotides. The amplicons were separated by agarose gel electrophoresis, purified, and sequenced to confirm the precise exon deletion from mouse *Rgr-d* mRNA. The mRGR-Fwd primer was used to obtain sequence from exon III to the beginning of exon VII of the mouse *Rgr* mRNA.

## Antibodies

Affinity-purified rabbit polyclonal antipeptide antibodies against RGR-d (DE21 antibody),[20] human RGR (DE7 antibody),[19,20] and the carboxyl terminus of mouse RGR (mcDE5 antibody)[37] were produced and authenticated, as described previously. Purified rat anti-mouse CD31 (number 557355) was obtained from BD Biosciences (San Jose, CA). Goat anti-rat IgG (H+L) secondary antibody conjugated to Alexa Fluor 488 (number A11006) was purchased from Life Technologies Corp. (Foster City, CA).

## Western Blot Assay

Protein samples were prepared from whole eyes of euthanized mice. The lenses were removed and eyecups were homogenized in 50 mmol/L sodium phosphate buffer (pH 6.5), 250 mmol/L sucrose, 1 mmol/L EDTA, and 1 mmol/L phenylmethylsulfonyl fluoride with a Brinkmann polytron. The homogenates were centrifuged at 800 × *g* for 5 minutes at 4°C, and the resultant supernatants were centrifuged at 100,000 × *g* for 30 minutes at 4°C to sediment membranes. The samples were resuspended in 200 μL of homogenization buffer and stored at −75°C until analyzed. Equal amounts of proteins were denatured and reduced in Laemmli sample buffer, separated by electrophoresis in 12% SDS-polyacrylamide gels [25 mmol/L Tris base, 192 mmol/L glycine, and 0.1% (w/v) SDS], and then transferred to 0.2-μm Immun-Blot polyvinylidene difluoride membranes (Bio-Rad Laboratories, Hercules, CA). The blots were blocked by incubation in 5% nonfat milk, or 3% gelatin, in phosphate-buffered saline (PBS), probed with affinity-purified mcDE5 primary antibody at ambient temperature, washed, and incubated with an anti-rabbit IgG

secondary antibody that was conjugated to horseradish peroxidase. mcDE5 is a rabbit polyclonal antibody that is directed against the carboxyl terminus of mouse RGR. Primary and secondary antibodies were suspended in 0.1% Tween-20 in PBS. Membrane washes were performed using 0.1% Tween-20 in PBS. Immunoreactive antigens were detected by chemiluminescence using the SuperSignal West Femto substrate (Pierce Biotechnology, Rockford, IL). Chemiluminescence was documented with the Bio-Rad ChemiDoc XRS+ Gel Imaging System (Bio-Rad Laboratories).

### Human Donor Eye Tissue

All experiments and procedures were conducted in compliance with applicable regulatory guidelines at the University of Southern California and the principles of human research subject protection in the Declaration of Helsinki. Postmortem eyes were obtained from the Doheny Eye and Tissue Transplant Bank (Los Angeles, CA) or the National Disease Research Interchange (Philadelphia, PA) and processed within 36 hours of the time of death. Tissues for frozen sections were dissected from the central retina and were fixed with 4% paraformaldehyde in PBS (D-5652; Sigma-Aldrich, St. Louis, MO) for 4 to 6 hours at 4°C and then infiltrated overnight with 30% sucrose in PBS. The RPE-choroid complex was dissected from the sclera, embedded in OCT compound (Miles, Elkhart, IN), and frozen. The frozen tissues were sectioned with a cryostat at −20°C to a thickness of 5 to 8 μm and mounted on Superfrost/Plus slides (Fisher Scientific, Pittsburgh, PA). Tissue blocks and slides were stored at −80°C.

### Immunofluorescence Staining

After euthanasia of mice, the eyes were enucleated, and the corneas were removed immediately under a dissection microscope while the eyes were immersed in PBS. The eyecups were then fixed with 4% paraformaldehyde for 40 minutes. The lenses were removed, and the eyecups were fixed for another 4 hours. The eyecups were infiltrated with 12% to 14% sucrose for 3 to 5 hours and then 25% to 28% sucrose overnight at 4°C. The tissues were then embedded in OCT compound and frozen over liquid nitrogen. Frozen tissue sections with a thickness of 8 μm were prepared with a cryostat at −15°C.

For immunostaining, retina sections were treated with cold acetone for 5 minutes, washed with 0.1% Tween-20 in PBS, and then incubated for 1 hour at room temperature with blocking buffer, consisting of 0.2% dodecylmaltoside, 5% (v/v) normal goat serum, and 3% (w/v) bovine serum albumin in PBS. The samples were then incubated with the primary antibody at 4°C overnight, washed with 0.1% Tween-20 in PBS, and incubated with fluorescent fluorescein isothiocyanate (FITC)—conjugated secondary antibody for 1 hour at room temperature. The tissue sections were washed and immersed with antifade mounting medium containing propidium iodide or DAPI (Vector Laboratories, Burlingame, CA). The slides were viewed with a Zeiss LSM 710 confocal microscope (Carl Zeiss Meditec, Inc., Dublin, CA) or an Olympus U-RFL-T fluorescence microscope (Olympus Corp., Center Valley, PA).

### Ocular Histology

Mouse eyes were immersed overnight in Davidson fixative and then transferred into 10% buffered formalin. The corneas and lenses were either removed or kept before embedding the eyes in paraffin. The formalin-fixed, paraffin-embedded tissue sections were cut at 5 μm thickness using a rotary microtome. Hematoxylin-eosin staining was performed, and the slides were scanned and imaged using the Aperio Scanscope Model CS (Leica Biosystems, Buffalo Grove, IL). The thickness of the retina, outer segment, outer nuclear layer (ONL), and inner nuclear layer was measured with the build-in ruler tool of Aperio ImageScope 12.1.0.5029 (Leica Biosystems). All the images were measured at the middle of an anterior quadrant or at the middle of a posterior quadrant of the retina to represent the peripheral and central areas of the retina, respectively. Total ganglion cell nuclei of the anterior quadrant (periphery) and posterior quadrant (central) of the retinas were counted.

### Postmortem Fundus Image

The corneas and lenses of the eyes from euthanized mice were removed after fixation with 1/2 Karnovsky fixative. The eyecups were placed on PBS-immersed filter papers and viewed under a dissection microscope. The images were taken with an iPhone X (Apple Inc., Cupertino, CA) through the eyepiece of the microscope using Ullman Indirect (*http://www.ullmanindirect.com/*, last accessed April 25, 2019; available for both iPhone and Android).

### Electron Microscopy

Eyes were removed from euthanized mice, and the corneas were excised immediately. The eyes were fixed with 1/2 strength Karnovsky fixative for 40 minutes, and the lenses were then removed. The eyecups were further fixed overnight. Under the dissection microscope, rectangular pieces with a length of 2 mm were dissected from the eyecups near optic disk or ora serrata. The pieces were stored in 1/2 Karnovsky fixative at 4°C until further processing. Post-fixation was performed in 1% aqueous osmium tetroxide, reduced with ferrocyanide, and the tissues were *en bloc* stained with uranyl acetate at 4°C overnight. Next, the pieces were dehydrated with 10%, 25%, 50%, 70%, 90%, and 3 × 100% acetone for 30 minutes each time. The tissues were infiltrated with 25%, 50%, 75%, and 2 × 100% uncatalyzed Spurr resin in acetone for 24 hours each, and then embedded and polymerized in fully catalyzed Spurr

resin. Alternatively, the pieces were dehydrated with 50%, 70%, 90%, 95%, and 100% ethanol for 30 minutes each time, treated with propylene oxide and epoxy resin, and then embedded and polymerized in epoxy resin. The tissue blocks were trimmed, and areas of interest were identified under an optical microscope. FEI Tecnai Spirit transmission electron microscope (FEI Company, Hillsboro, OR), JEOL JEM-2100 (JEOL, Peabody, MA), or Zeiss EM-10 (Carl Zeiss, Inc., Thornwood, NY) was used to view 50- to 70-nm ultrathin sections and for imaging.

## Choriocapillaris Quantification

Immunofluorescence images were taken by confocal microscope, and montages of whole eye cross-sections were aligned with Photoshop CC (Adobe, Inc., San Jose, CA).

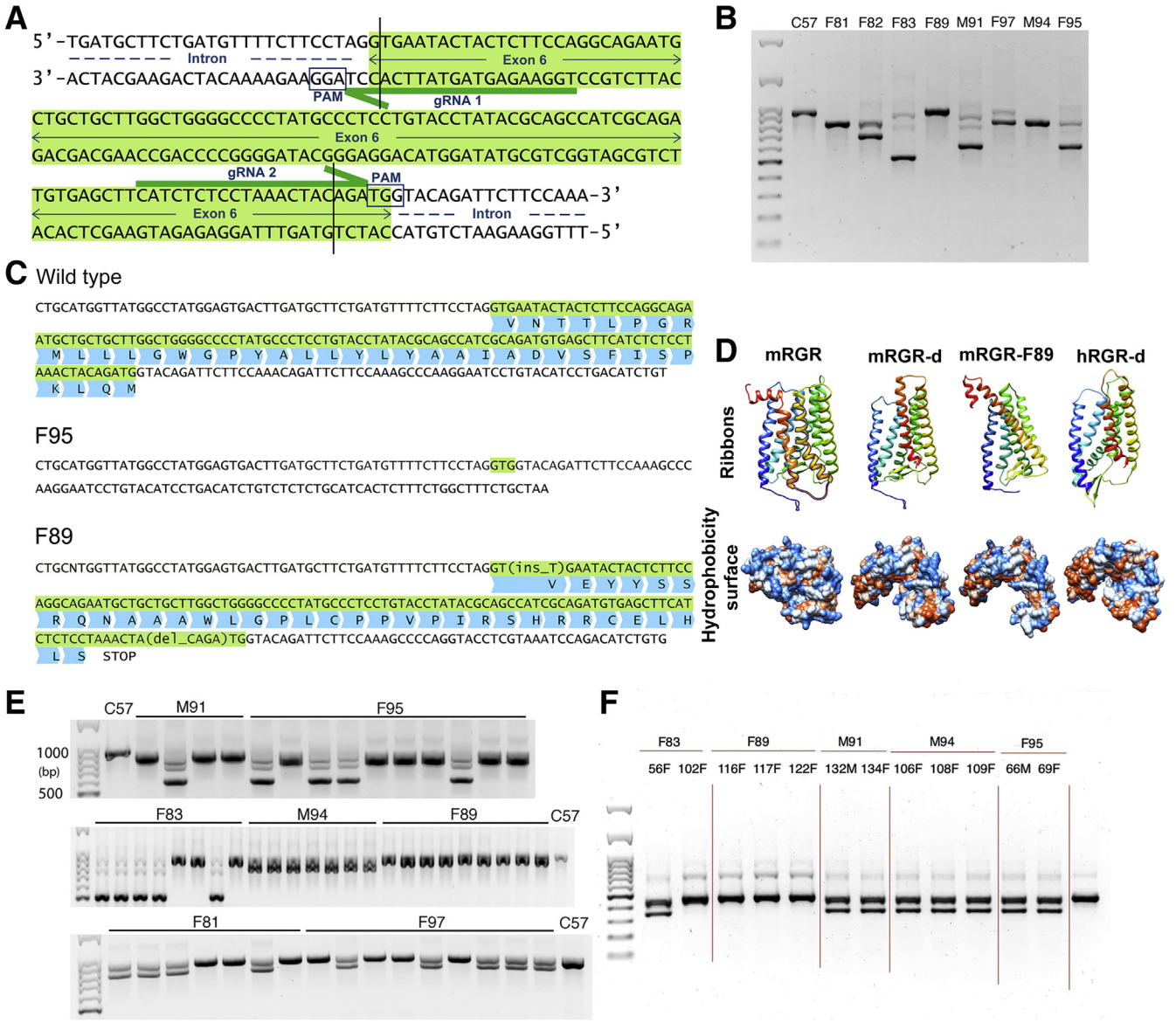


**Figure 1** Mouse *Rgr* gene editing. **A:** RGR-d mutant mice were generated by targeting both splice sites of exon VI (shaded green) of the mouse *Rgr* gene using a CRISPR gene-editing method. Target sequences of the two guide RNAs (gRNAs; **half green arrows**) are shown with required protospacer adjacent motif (PAM) sequence (boxed text). The approximate cut sites (**vertical lines**) are close to the exon-intron junctions. **B:** The founder mice and a control C57BL/6J mouse were analyzed by the amplification of genome segments using primers flanking exon VI. Seven mice that exhibited smaller bands were considered to have the exon VI deleted. **C:** Nucleotide sequencing showed that exon VI in mouse line F95 had been deleted with only three nucleotides (GTG) of the exon remaining (shaded green). In mouse line F89, there were two frameshift mutations in a transcript that encoded a truncated RGR with altered carboxyl terminus. Translated amino acid sequences of exon VI and the altered frameshift mutant are shaded blue. **D:** The three-dimensional model structures of full-length mouse RGR (mRGR), the mutant RGR proteins in mouse lines F95 (mRGR-d) and F89 (mRGR-F89), and human RGR-d (hRGR-d) were obtained from the online program Phyre 2. **E:** Genotype analysis of $F_1$ offspring from matings between founder mice and wild-type DBA/2J mice. **F:** Analysis of mouse *Rgr* mRNA in heterozygous $F_1$ offspring of founder mice by reverse transcription and PCR amplification. DNA fragments of approximately 445 bp and approximately 331 bp were amplified from the mutant mice. The approximately 331-bp amplicons from F95 and several other lines were sequenced and found to contain exactly the 114-bp deletion of exon VI. DNA markers and amplicons from a control C57BL/6J mouse were loaded in the leftmost and rightmost lanes, respectively.

The method of quantification was similar to that described previously.[38] The fluorescence of the retina, large choroidal vessels, and extraocular muscles was deleted. The threshold level of each image was adjusted to the same value to enhance the intensity for quantification. ImageJ software version 1.52a (NIH, Bethesda, MD; *https://imagej.net/Welcome*, last accessed July 9, 2019) was used to perform the quantification of the fluorescent intensity. The procedures were as follows: i) open an image and convert it into 8-bit; ii) invert the image; iii) calibrate the image; iv) adjust the threshold; and v) measure the area and area fraction. Because the mean gray value was low due to the small area of choriocapillaris compared with the background, the area fraction (percentage area) was used to represent the immunofluorescence intensity.

## Statistical Analysis

The *t*-test with Welch correction was used to analyze the following measurements of different groups of mice: i) thickness of the retina, outer segment, ONL, and inner nuclear layer; ii) nuclei layers of ONL and inner nuclear layer; iii) ganglion cell count per quadrant of retina; and iv) area fraction of CD31 immunofluorescence intensity. Significant differences were assumed for $P < 0.05$.

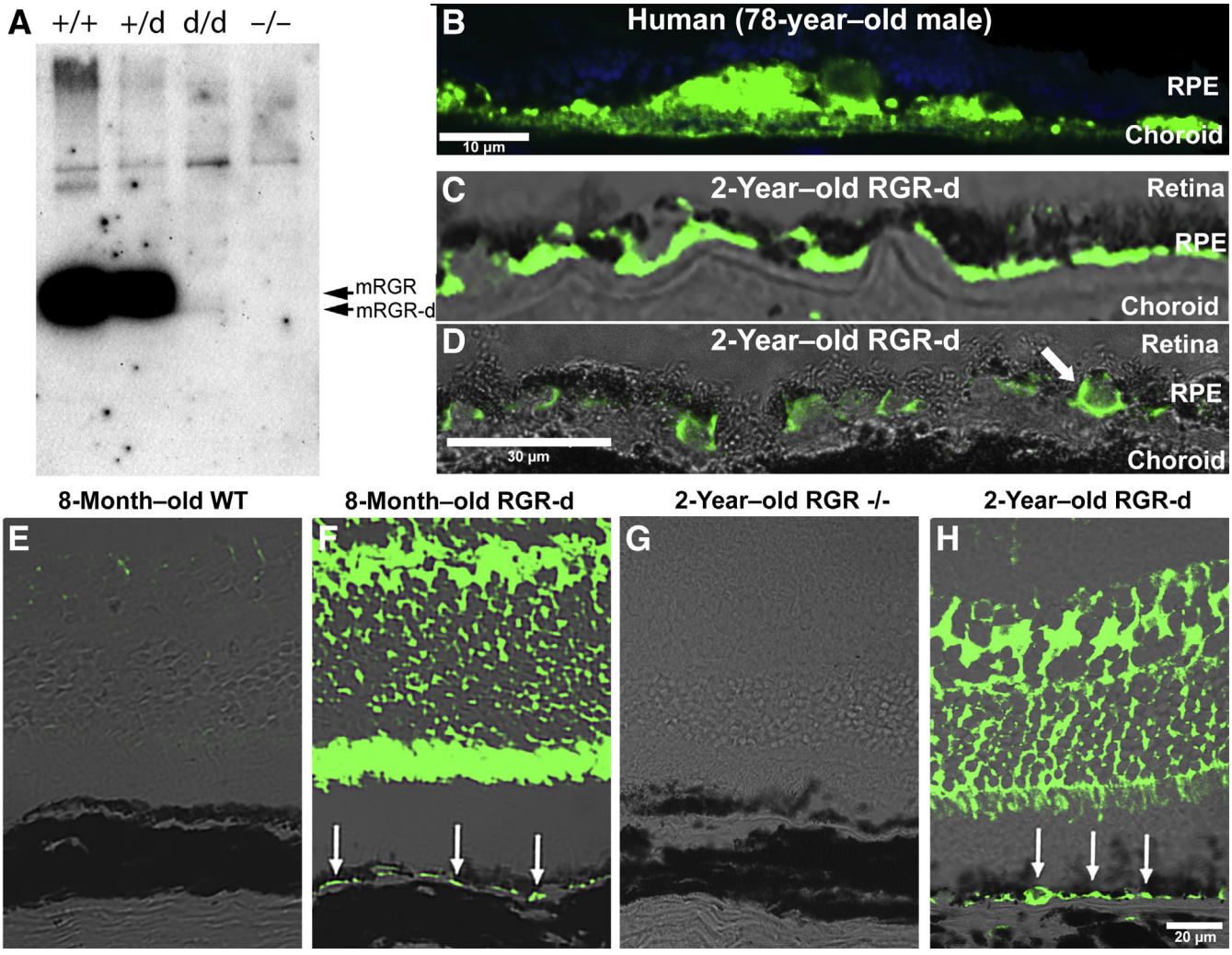


**Figure 2** RGR-d expression and basal deposits from human and mouse retinal pigment epithelium (RPE). **A:** Western immunoblot assay of RGR and RGR-d proteins in mouse eyes from 8-week–old wild-type (WT; +/+), heterozygous (+/d), homozygous RGR-d mice (d/d), and $RGR^{-/-}$ knockout mice (−/−). **B**–**H:** Expression of RGR-d was detected also by immunofluorescence staining of retina sections using RGR-d–specific antibody DE21 and secondary anti-rabbit IgG conjugated to fluorescein isothiocyanate. **B:** Localization of human RGR-d in basal deposits in an RPE-choroid section from a 78-year–old male donor. **C** and **D:** Localization of mouse RGR-d at the basal boundary of the RPE in older RGR-d mice (d/d). The images show superimposed fluorescence and phase contrast images. The localization of RGR-d coincided with the basolateral plasma membrane in some of the RPE cells (**arrow**). **E**–**H:** RGR-d immunofluorescence was not detected in the RPE or retina of 8-month–old wild-type or 2-year–old $RGR^{-/-}$ mice other than background staining. RGR-d expression was found in both RPE (**arrows**) and retina of 8-month–old and 2-year–old RGR-d mice (d/d). In the RPE, RGR-d was concentrated mainly near the basal region. Magnification is the same for panels **C** and **D**, and that for panels **E**–**H**. Scale bars: 10 μm (**B**); 30 μm (**C** and **D**); 20 μm (**E**-**H**).

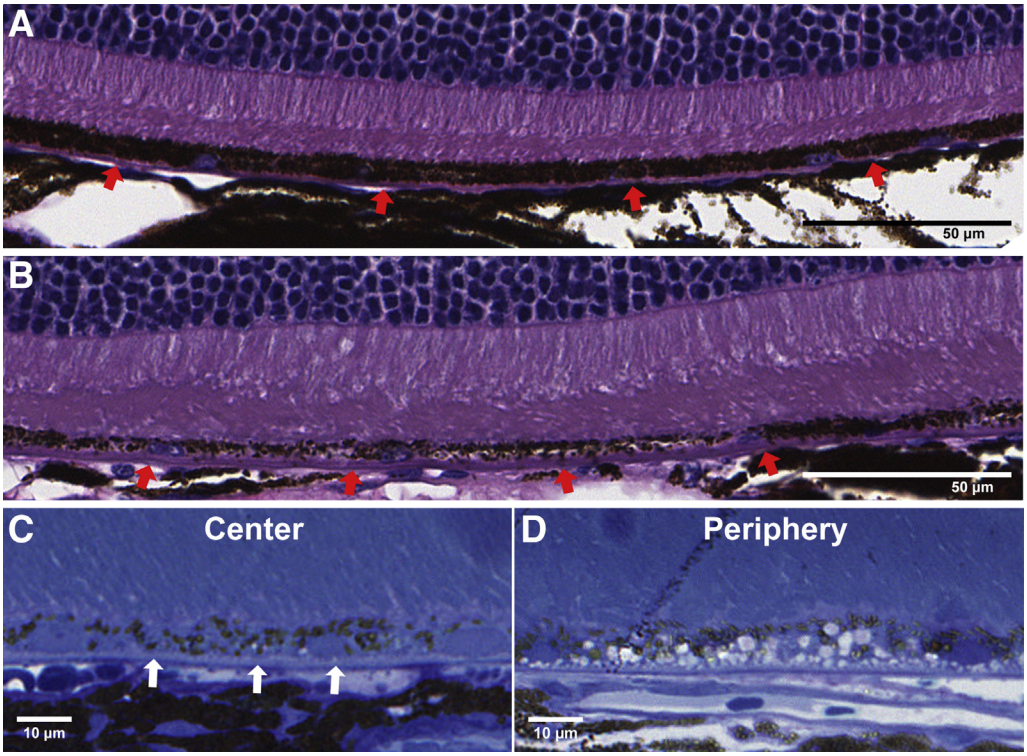


**Figure 3** Old RGR-d mice showed retinal pigment epithelium (RPE) abnormalities and sub-RPE bands of eosinophilic material at the light microscopic level. **A** and **B:** Formalin-fixed, paraffin-embedded sections of retinas from approximately 21-month-old $RGR^{-/-}$ (**A**) and RGR-d (d/d) **B**) mice were stained with hematoxylin-eosin (H&E). **C** and **D:** Epoxy-embedded thin sections from an RGR-d (d/d) mouse were stained with toluidine blue. Typically, old RGR-d mice develop a thickening of the Bruch membrane or confluent band of sub-RPE material in comparison to old $RGR^{-/-}$ mice. This distinctive sub-RPE layer is eosinophilic (**red arrows**) or pale (**white arrows**) on staining with H&E or toluidine blue, respectively. Prominent RPE cell abnormalities in old RGR-d mice are seen often. **C** and **D:** Severe pathologic changes include RPE atrophy, cell hypertrophy (**C**), or extreme vacuolization (**D**). Scale bars: 50 μm (**A** and **B**); 10 μm (**C** and **D**).

## Modeling of Protein Three-Dimensional Structure

The three-dimensional structures of mouse full-length RGR, RGR-d, and RGR-F89, as well as human RGR-d, were predicted using online software Phyre 2.0 (*http://www.sbg.bio.ic.ac.uk/servers/phyre2/html/page.cgi?id=index*, last accessed March 1, 2021). The modeling was based on the homology between the proteins of interest and human rhodopsin with a >98% confidence. Molecular graphics and analyses were performed with University of California San Francisco Chimera 1.13.1 (*https://www.cgl.ucsf.edu/chimera/*, last accessed March 2, 2021) developed by the Resource for Biocomputing, Visualization, and Informatics at the University of California, San Francisco, with support from NIH P41-GM103311. Chimera was used to further analyze the protein structures generated by Phyre 2, including ribbons and hydrophobicity surface.

## RGR and RGR-d Expression Vectors

pFLAG-hRGR and pFLAG-hRGR-d DNA expression vectors were constructed, as described previously.[32] Human RGR and RGR-d cDNAs were cloned into the pFLAG-CMV-4 vector (Sigma-Aldrich) to generate FLAG-RGR and FLAG-RGR-d fusion proteins.

## DNA Transfection and Production of Stable Cell Lines

COS-7 and LN-229 cells were cultured in Dulbecco's modified Eagle's medium supplemented with 10% fetal bovine serum. ARPE-19 cells were cultured in Dulbecco's modified Eagle's medium/Ham F12 (1:1) medium supplemented with L-glutamine, penicillin/streptomycin, and 10% fetal bovine serum. All cell lines were incubated at 37°C in a humidified atmosphere of 95% air and 5% carbon dioxide. Stable transformants were established by plasmid DNA transfection using Lipofectamine 2000 (Invitrogen), per manufacturer's guidelines for 6-well culture plates. The cells were transfected with pFLAG-hRGR, pFLAG-hRGR-d, or empty control pFLAG-CMV-4 vectors. Selection for the presence of the G418 resistance gene was performed by supplementing COS-7 and LN-229 culture media with 600 μg/mL G418 (Gibco BRL, Carlsbad, CA) and ARPE-19 media with 1200 μg/mL G418. All DNA-transfected cells and sham-transfected control cells (transfection without DNA vector) were grown in selection level G418 until all

control cells without DNA vector had died. Thereafter, all cell lines were maintained continuously in 300 μg/mL G418.

### Cell Culture Doubling Time

Equal numbers of parental ARPE-19 or COS-7, or stable transformants of ARPE-19 or COS-7 that expressed RGR or RGR-d, were cultured in 4- or 8-well chamber slides (BD Biosciences, Bedford, MA). The bottoms of the chamber slides were marked uniformly in three to four separate regions with a circular stamp. The cells were visualized using an inverted phase contrast microscope, and cells in each marked region of the wells were counted daily. Cell doubling time was calculated during the logarithmic phase of growth.

### Immunofluorescence Labeling of Cultured Cells

LN-229 stably transformed cells were cultured on 8-well chamber slides (BD Biosciences, Bedford, MA) for immunofluorescence analysis of FLAG-RGR and FLAG-RGR-d fusion proteins. The nonpolarized LN-229 cells were fixed with 2% paraformaldehyde in PBS and then ice-cold methanol for 5 minutes each. The samples were treated with blocking buffer that consisted of 0.2% dodecylmaltoside, 5% (v/v) normal goat serum, and 3% (w/v) bovine serum albumin in PBS. The slides were incubated overnight at 4°C with first primary anti-FLAG antibody (Sigma, St. Louis, MO) diluted in 0.2% dodecylmaltoside in PBS and subsequently incubated with anti-mouse FITC-conjugated secondary antibody for 1 hour at room temperature. After washing, the procedure was repeated with anti-calnexin antibody and then anti-rabbit IgG antibody conjugated to Cy3. Control slides were treated in parallel, except that the primary antibodies were omitted from the binding buffer. The sections were mounted using VECTASHIELD Mounting Medium with DAPI (Vector Laboratories). The immunofluorescence from secondary antibodies conjugated to FITC or Cy3 was viewed with a PerkinElmer 6-line Spinning Disk Laser Confocal Microscope (PerkinElmer, Waltham, MA).

## Results

### Mouse *Rgr* Gene Editing

RGR mutant mice were generated by directed mutation of the splice sites at each end of exon VI of the mouse *Rgr* gene. Splice sites were excised by multiplex gene editing using CRISPR methods (Figure 1). A pair of single gRNAs, that target the two splice sites of mouse *Rgr* exon VI (Figure 1A), and Cas9 mRNA were microinjected into single-cell wild-type B6D2F1/J embryos.

Mice with mutation of or near either the 5′ or 3′ splice site, both splice sites, or with total deletion of exon VI were

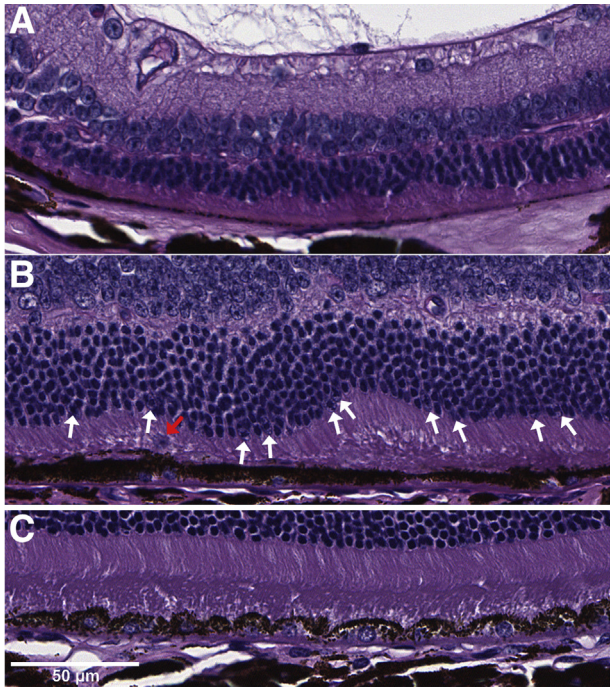


**Figure 4** Old RGR-d mice showed pathologic changes in the retina and retinal pigment epithelium (RPE). Formalin-fixed, paraffin-embedded sections and hematoxylin-eosin staining were performed on retinas from approximately 2-year—old RGR-d mice and were analyzed by light microscopy. **A:** Cell fusion of inner nuclear layer and outer nuclear layer (ONL) was observed in the peripheral retina. Depigmentation and atrophy of RPE was seen in some areas. **B:** Pyknosis was observed in multiple cells of the ONL, especially in the cells that were closest to the RPE layer (**white arrows**). Abnormal cell nucleus was found between the outer segment and RPE (**red arrow**). Outer segments were misaligned, and a subretinal deposit distorted the position of the ONL. **C:** RPE cell hypertrophy was also observed. Magnification is the same for panels **A**—**C**. Scale bar = 50 μm (**A**—**C**).

expected. One litter of eight viable pups was analyzed, and these founder mice were designated F81, F82, F83, F89, M91, M94, F95, and F97. Seven of the founders had visible deletions within the *Rgr* gene, as indicated by smaller amplicon bands from genotype analysis (Figure 1B). The deletions were of various sizes.

The amplicons were sequenced to confirm gene editing of the splice sites, as well as to characterize the deletions or insertions in the region of exon VI. The PCR products were purified, and the DNA was sequenced using a primer within the intron at the 5′ end of exon VI. In mouse line F95, the 5′ and 3′ intron splice sites were intact; however, there was a deletion of all of exon VI, except three nucleotides (GTG) (Figure 1C). In mouse line F89, the 5′ and 3′ intron splice sites were intact; however, there was a frameshift insertion of one nucleotide (T) and a revert-to-frame deletion of four nucleotides (CAGA) at the 5′ and 3′ ends of exon VI, respectively (Figure 1C). In this mouse line, the mutant RGR isoform, referred to as RGR-F89 (AAC69836: p.Asn212Glufs*34), was truncated because of a stop codon following an altered frameshift sequence of 33 amino acids. Models of the mouse and human RGR-d proteins show a

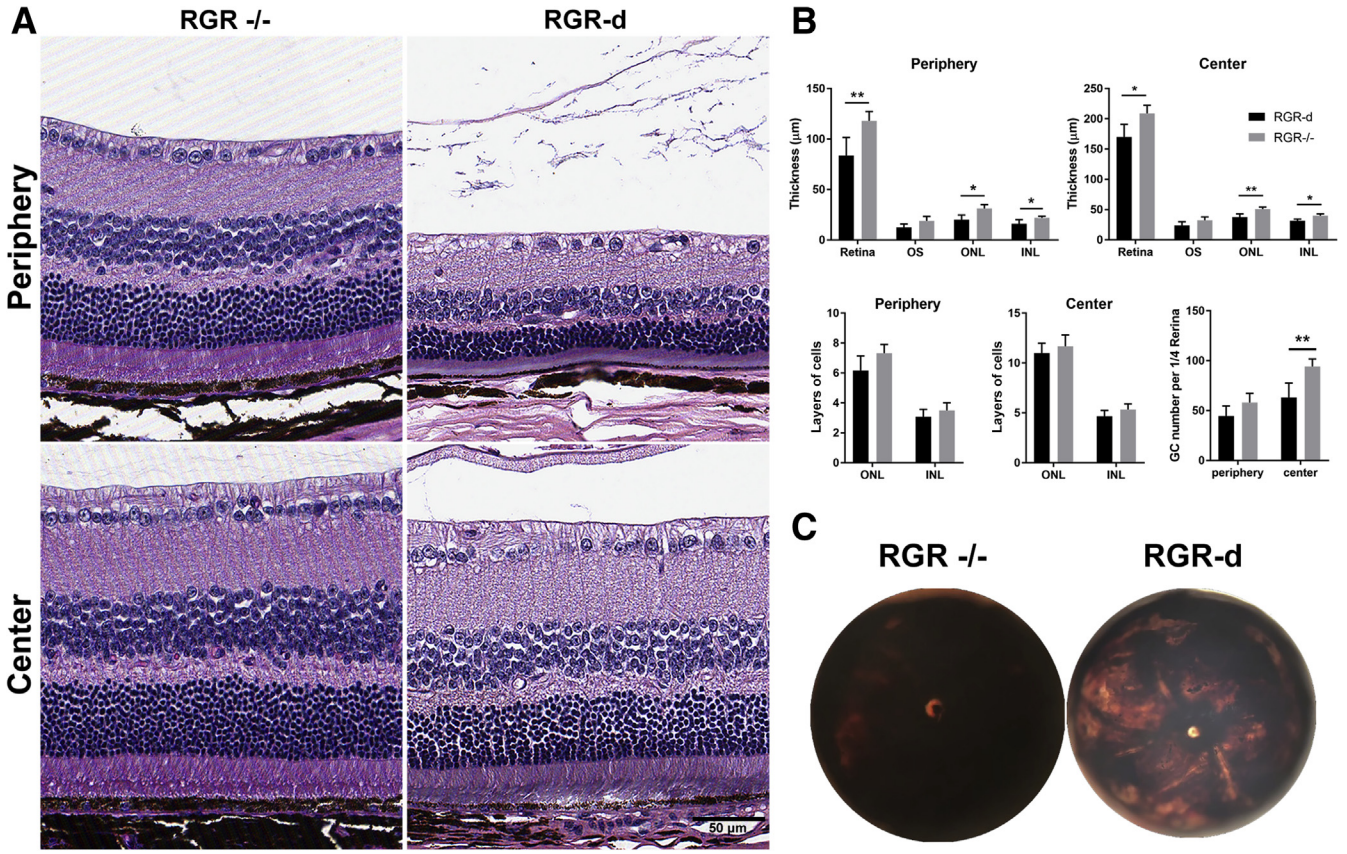


**Figure 5** RGR-d mice presented slow retinal degeneration. The retinas in old RGR$^{-/-}$ and RGR-d mice (31 months old) were analyzed. Formalin-fixed, paraffin-embedded sections crossing the optic nerves were prepared with hematoxylin-eosin staining to observe retinal morphology. **A:** RGR$^{-/-}$ mice without full-length RGR or RGR-d showed normal morphology of the retina and retinal pigment epithelium. In contrast, RGR-d mice showed retinal degeneration, especially in the peripheral area. **B:** The thickness of the retina, outer nuclear layer (ONL), and inner nuclear layer (INL) in both peripheral and central areas were narrower in the RGR-d mice than in RGR$^{-/-}$ mice. The layers of cell nuclei in the ONL and INL were lower in RGR-d than in RGR$^{-/-}$ mice, but the differences in counted layers were not significant ($P > 0.05$). The number of ganglion cell nuclei in the central retina was significantly lower in RGR-d mice than in RGR$^{-/-}$ mice. **C:** The gross morphology of the fundus of 31-month—old RGR$^{-/-}$ and RGR-d mouse eyecups under dissection microscope after the cornea and lens were removed. Multiple depigmentation and lesion-appearing areas were found in RGR-d mice. These lesions appear to become more severe during aging in RGR-d mice. $n = 5$ (**B**). $^{*}P < 0.05$, $^{**}P < 0.01$. Scale bar = 50 μm (**A**). OS, outer segment.

sterically inverted former transmembrane domain VII and overall similarity, whereas the RGR-F89 protein contained only five transmembrane domains with altered structure after transmembrane domain IV (Figure 1D). Hydrophobicity surface indicates that the normal RGR forms the structure of a potential G-protein—coupled receptor, whereas both RGR-d and RGR-F89 proteins and human RGR-d deviate strongly and fail to form such a structure.

## Mouse *Rgr-d* mRNA and Protein Expression

The genotype of the $F_1$ progeny was analyzed to further differentiate the mutated *Rgr* alleles (Figure 1E). Various splice-site mutations, or whole deletion of exon VI, may result in targeted exon skipping in the mouse *Rgr* mRNA. To confirm the presence of *Rgr-d* mRNA in the $F_1$ mice, *Rgr* transcripts were assayed by means of reverse transcription and PCR. The reverse transcriptase reaction was performed using the mouse RGR-specific mRGR-Rev primer and eyecup total RNA. A pair of PCR primers, mRGR-Rev and mRGR-Fwd, were used to amplify expected 445- or 331-bp fragments that correspond to the intact *Rgr* and truncated *Rgr-d* mRNAs, respectively. The results of the reverse transcriptase and PCR assay indicated that DNA fragments of approximately 445 bp and approximately 331 bp were amplified from the mutant mice (Figure 1F). The approximately 331-bp PCR fragment from F95 and several other lines was excised and sequenced, and it was found to contain the precise 114-bp deletion of exon VI. Only mouse line F95 was maintained for breeding.

Next, the expression of RGR and RGR-d proteins in 8-week—old wild-type and mutant mice was investigated by detection with the mcDE5 antibody, which is directed against the identical C-terminal peptide sequence of mouse RGR and RGR-d (Figure 2A). Full-length RGR was readily detectable by Western immunoblot of eyecup proteins from wild-type (+/+) and heterozygous mice (+/d), but completely absent from the eyecup proteins from homozygous RGR-d mice (d/d) and RGR knockout mice (−/−)

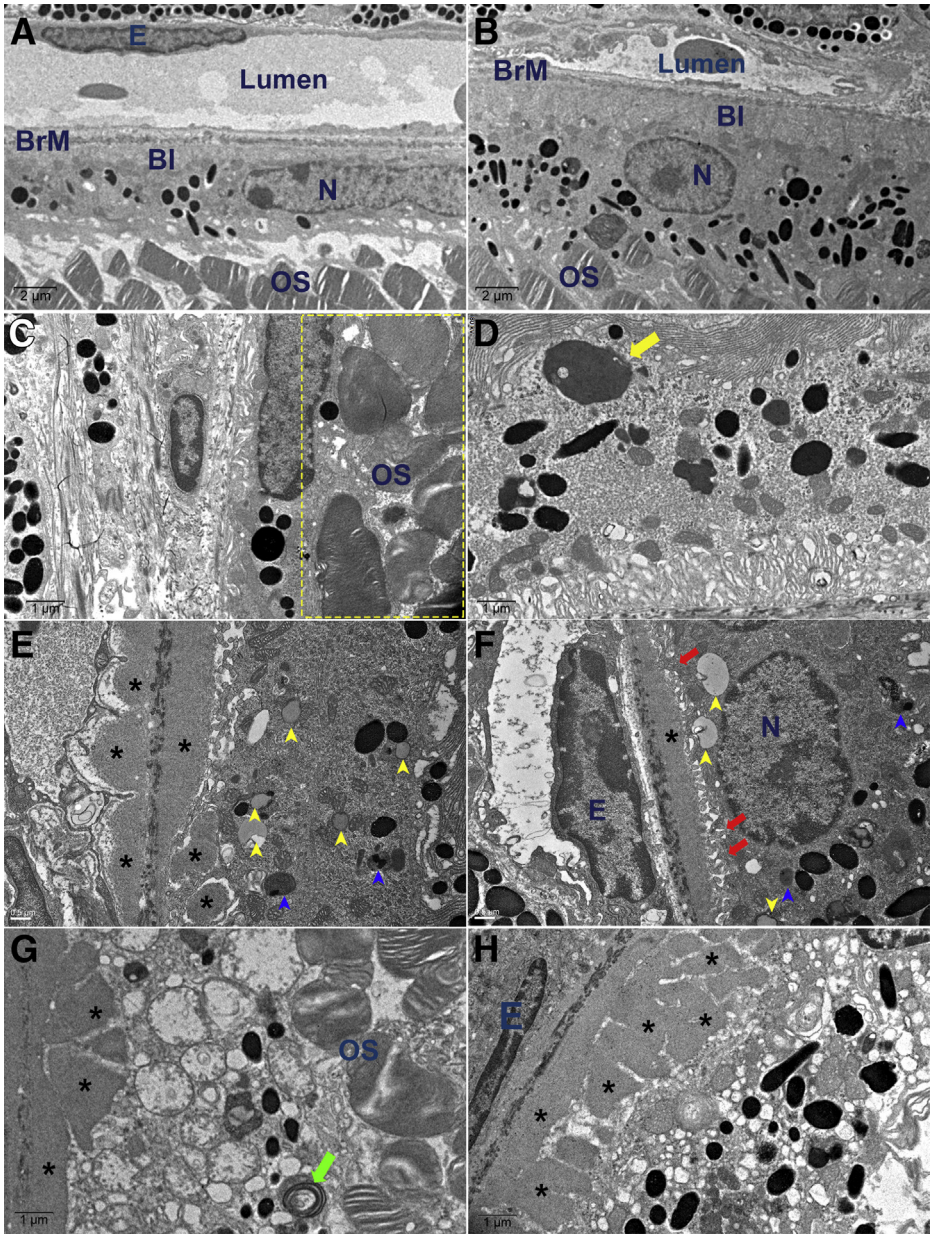


**Figure 6** Ultrastructure of the retinal pigment epithelium (RPE), Bruch membrane (BrM), and choriocapillaris in RGR-d mice. **A**—**H:** Electron microscopy of retinas from an 11-month—old wild-type mouse (**A**), a 23-month—old $RGR^{-/-}$ mouse (**B**), and RGR-d (d/d) mice at different ages (**C**—**H**), as follows: 10 months old (**C**), 16 months old (**D**), 21 months old (**E** and **F**), and 27 months old (**G** and **H**). **A** and **B:** Control wild-type and $RGR^{-/-}$ mice showed normal RPE—Bruch membrane—choriocapillaris structures. **C:** In the 10-month—old RGR-d mouse, misaligned and partially degenerated outer segment (OS) was observed (**yellow boxed area**). **D:** In the 16-month—old RGR-d mouse, normal basal infoldings and large phagosome-like granules (**yellow arrow**) were seen in the RPE. **E** and **F:** In the 21-month—old RGR-d mouse, a thickened Bruch membrane was prominent and protrusions of diffuse granular deposits (**asterisks**) projected toward either the RPE or the choroid. Lipofuscin (**yellow arrowheads**), melanolipofuscin (**blue arrowheads**), and disorganized basal infoldings (**red arrows**; **F**) were observed in the RPE. **G** and **H:** In the 27-month—old RGR-d mouse, severe vacuolization and multilamellar bodies (**green arrow**) developed in the RPE. Diffuse granular deposits were seen throughout the Bruch membrane, and these dense masses extended deep toward the RPE (**asterisks**). Scale bars: 2 μm (**A** and **B**); 1 μm (**C**, **D**, **G**, and **H**); 0.5 μm (**E** and **F**). BI, basal infoldings; E, endothelial cell; N, RPE nuclei.

(Figure 2A). The RGR-d isoform was expressed at extremely low levels in homozygous RGR-d mice (d/d) relative to the abundance of normal RGR in wild-type (+/+) or heterozygous (+/d) mice (<1% of RGR in wild-type mice). To visualize RGR-d in RGR-d mice (d/d), the Western immunoblot was overexposed for the normal RGR protein.

## Basal RPE Deposits Containing RGR-d Protein

The expression of RGR-d protein in mutant mouse eyes was verified by immunofluorescence labeling (Figure 2, B—H). The RGR-d—specific antibody DE21 was used to detect expression and localization of RGR-d and to compare the targeting of RGR-d protein in mouse retina with that in

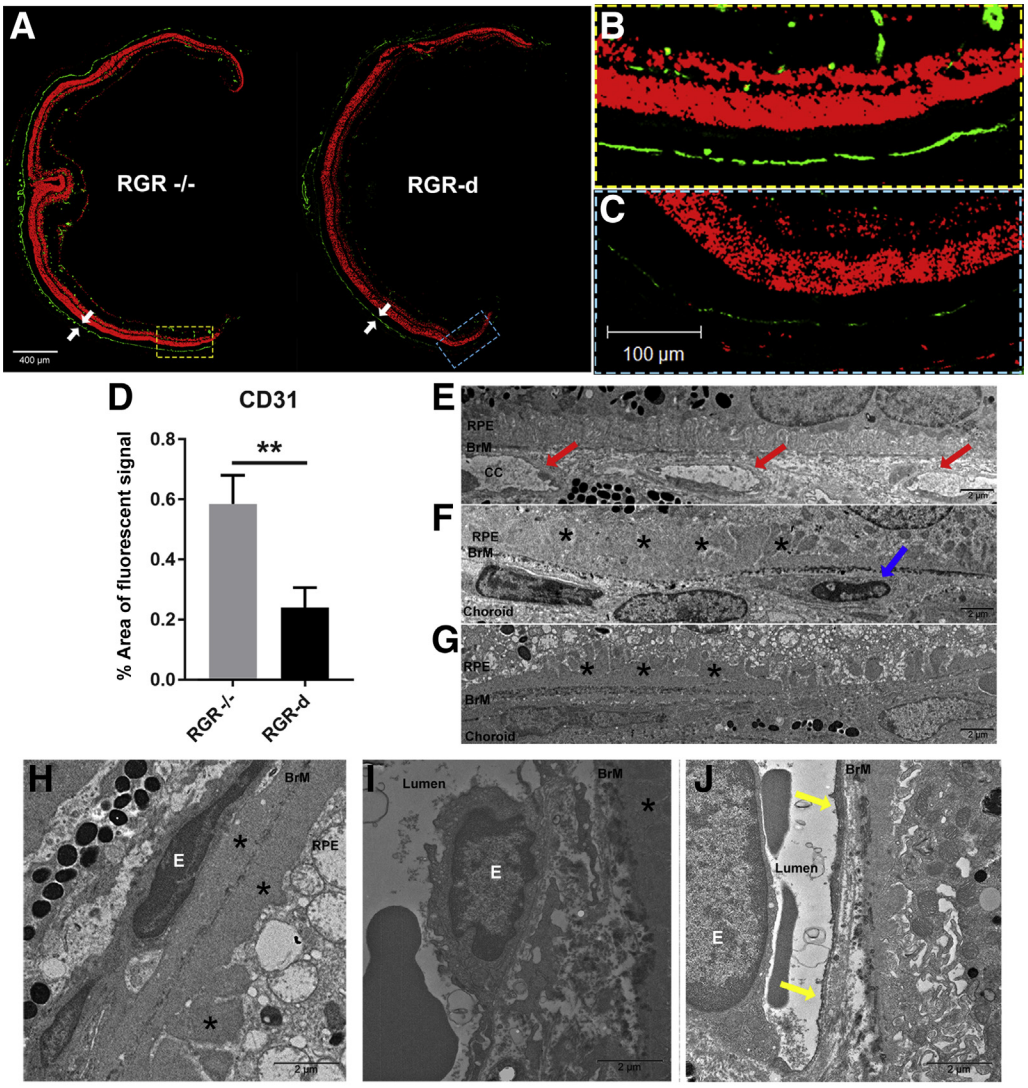


**Figure 7** Extensive loss of choroidal capillaries occurred in old RGR-d mice. Anti-CD31 antibody was used to label the choriocapillaris (CC) by immunofluorescence. **A:** CD31 immunofluorescence (**arrows**) in 21-month–old RGR-d (d/d) mice was less continuous and less intense than that in 22-month–old $RGR^{-/-}$ mice (green, CD31; red, propidium iodide). **A–C:** The higher magnification of **boxed areas** (**A**) shows CD31 immunofluorescence in $RGR^{-/-}$ (**B**) and RGR-d (**C**) mice. **D:** The CD31 expression that coincides with the choriocapillaris in RGR-d mice was significantly less continuous than that in $RGR^{-/-}$ mice. **E:** Electron microscopy of the choriocapillaris (**red arrows**) in an $RGR^{-/-}$ mouse. **F:** In RGR-d (d/d) mice, endothelial cells showed displaced nuclei with condensed chromatin (**blue arrow**), and shrunken lumens indicated capillary atrophy. Thick basal deposits (**asterisks**) under the retinal pigment epithelium (RPE) were seen (thickness $>$ 4 μm). **G:** Choroidal capillaries were absent over a large area in old RGR-d mice with the presence of RPE vacuolization, loss of basal infoldings, and abundant basal linear deposits (**asterisks**). **H:** Shrunken or degenerating endothelial cells (**E**) were found often with capillary lumens absent. Murine-type basal linear deposits (**asterisks**) were present in the inner and outer collagenous zones. **I:** Capillary with open lumen; however, the endothelial cell nucleus (**E**) is dislocated to the side of the Bruch membrane (BrM) in which diffuse grainy deposits (**asterisks**) were concentrated. **J:** Thickened cytoplasm of endothelial cells (**E**) along the inner wall of the choriocapillaris (**yellow arrows**) was associated with reduced fenestrations. $n = 3$ (**D**). $^{**}P < 0.01$. Scale bars: 400 μm (**A**); 100 μm (**B** and **C**); 2 μm (**E–J**). Magnification is the same for panels **B** and **C**.

human retina (Figure 2B). In older human retinas, basal deposits and drusen are consistently immunoreactive for RGR-d.[32,33] Significant RGR-d labeling was seen in both 8-month–old and 2-year–old RGR-d mice, but not in control wild-type or $RGR^{-/-}$ knockout mice (Figure 2, C–H). Specific FITC-immunofluorescence labeling was also absent in negative controls with primary antibody omitted (Supplemental Figure S1). As in the human donor eye (78/M), RGR-d was concentrated at intermittent foci at the basal side of mouse RPE. Moreover, the RGR-d foci were more extensive in the older RGR-d mice. RGR-d also trafficked to the basolateral plasma membrane in a few RPE cells and was found in Müller cells.

## Ocular Histology and Retinal Degeneration

The histology of normal and homozygous RGR-d mouse retinas was examined. At 2 weeks of age, little change was noted by light microscopy between the retinas of wild-type and RGR-d $F_2$ littermates. By 5 months of age, RPE cells in

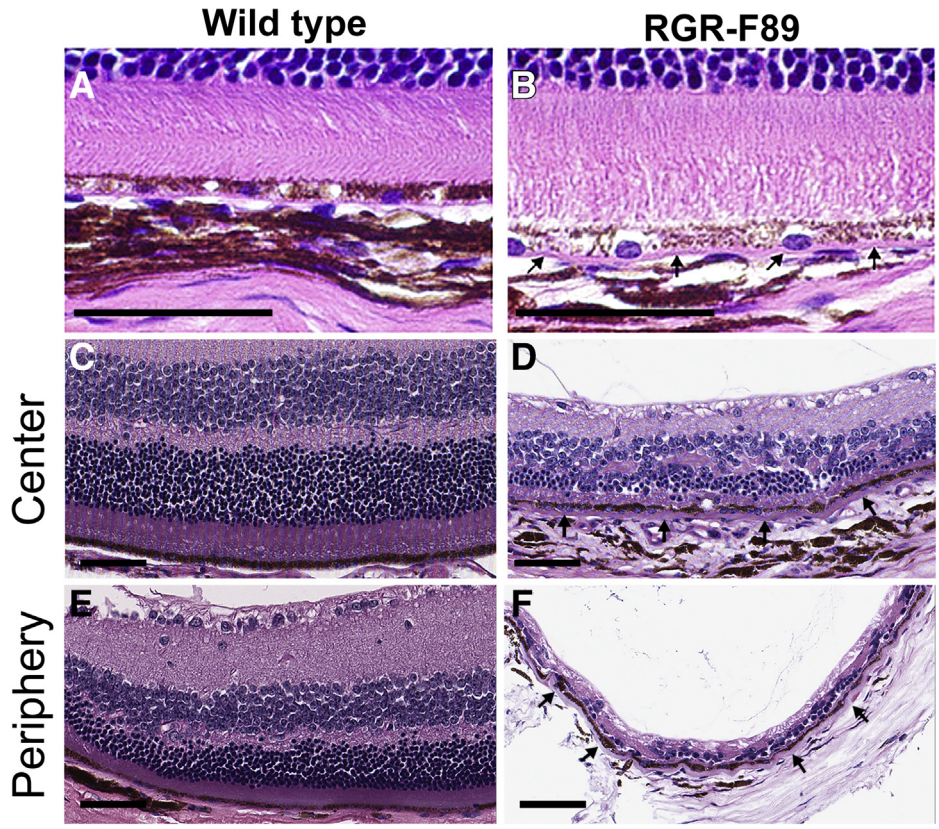


**Figure 8** Severe retinal degeneration in RGR-F89 mutant mice. **A**—**F:** Formalin-fixed, paraffin-embedded sections and hematoxylin-eosin staining were performed on eyes from wild-type (**A**, **C**, and **E**) and homozygous RGR-F89 (**B**, **D**, and **F**) mice. **A**—**F:** The mice were 3 months (**A** and **B**) or approximately 23 months (**C**—**F**) of age. **B:** In the 3-month—old RGR-F89 mouse, thick continuous eosinophilic tissue was seen beneath the retinal pigment epithelium (RPE; **arrows**). **D** and **F:** In the 23-month—old RGR-F89 mouse, the retina was noticeably degenerated throughout both central and peripheral areas, and an extremely thick confluent band of eosinophilic material was seen beneath the RPE (**arrows**). **D:** In the central area, the outer nuclear layer (ONL) and inner nuclear layer (INL) were degenerated severely and arranged disorderly. RPE cell degeneration was also remarkable. Pyknosis was seen in many cells in the ONL and some in the INL. **F:** In the peripheral area, the degeneration of the RGR-F89 mouse retina was nearly complete. The remnant cells of the INL and ONL were intermixed, and ganglion cells were lost completely. The thick confluent band of sub-RPE deposits extended throughout the peripheral retina. Scale bar = 50 μm (**A**—**F**).

RGR-d mice (d/d) showed apical displacement of intracellular pigment and appeared vacuolated compared with RPE cells in the wild-type littermate (Supplemental Figure S2).

For older mice, the histology of RGR-d (d/d) mouse retinas was compared with that of $RGR^{-/-}$ knockout mice (Figure 3). Aged $RGR^{-/-}$ mice were used as controls because old homozygous RGR-d mice might also be affected by the long-term absence of normal RGR opsin (Figure 3A). At 21 months of age, the RGR-d mice showed long basal bands of eosinophilic deposits (Figure 3, B and C), as well as RPE vacuolization (Figure 3D). RPE hypertrophy, subretinal distortion of the ONL, and pigmentary abnormalities were observed at the light microscopic level (Figures 3 and 4). Both histologic and ultrastructural features of RGR-d mice were associated with retinal degeneration apparent in old mice (Figure 5A). In comparison to age-matched $RGR^{-/-}$ knockout mice, 2-year—old RGR-d mice showed significant atrophy of the retinal layers, cell losses in the inner and outer nuclear layers, and ganglion cell loss evident in the peripheral retina (Figure 5, A and B). Patchy depigmentation of the fundus, especially the anterior portion, was characteristic of old RGR-d mice, nearly all of whom had opaque cataracts (Figure 5C). These pigmentary lesions in the fundus were more severe on aging in RGR-d mice. Unfortunately, only a rare example was found of a hard drusen-like basal deposit in a 10-month—old heterozygous RGR-d (+/d) mouse (Supplemental Figure S3).

## Ultrastructural Abnormalities of RGR-d Mice

The ultrastructure of the RPE and Bruch membrane was examined in an 11-month-old wild-type mouse (Figure 6A), 23-month-old $RGR^{-/-}$ knockout mouse (Figure 6B) and RGR-d mice at different ages (Figure 6, C—H). At the electron microscopic level, old RGR-d mice showed amorphous protrusions of granular mass deposits at the basal side of the RPE that were continuous with and within Bruch membrane (Figure 6, E—H). The diffuse granular deposits extended as much as 4 μm deep toward the RPE, and the dense masses projected toward the choroid. In old RGR-d mice, RPE cells showed complete absence of basal

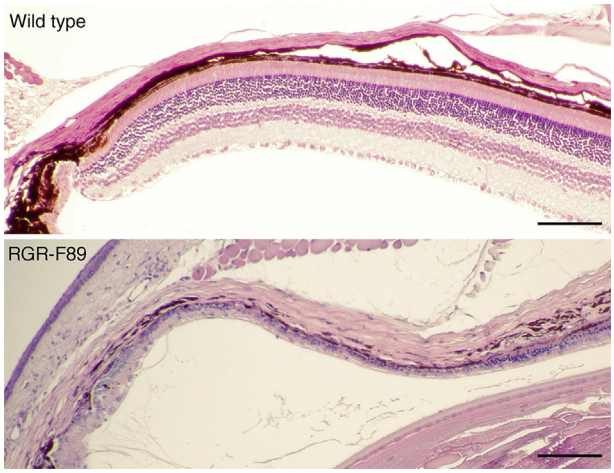


**Figure 9** Advanced retinal degeneration in RGR-F89 mutant mice from midperipheral region to the ora serrata. Low-magnification images of hematoxylin-eosin–stained formalin-fixed, paraffin-embedded retinal sections from the eyes of approximately 23-month–old wild-type (**top panel**) and homozygous RGR-F89 (**bottom panel**) mice. Even at this age, the retina from the wild-type mouse appeared largely normal. In contrast, the retina from the RGR-F89 mouse showed extreme and, in some areas, nearly complete degeneration. Scale bar = 100 μm.

infoldings and severe vacuolization (Figure 6, G and H). Membrane-bound microvesicles and organelles similar to multilamellar bodies with concentric membrane layers were observed inside RPE cells. Degeneration of the choriocapillaris was evident in these mice, as the internal wall of the endothelial cells along Bruch membrane was often overtly thick and vacuolated with consequent loss of fenestrations and anteriorly displaced nuclei (Figure 6, F and H).

## Choriocapillaris Degeneration in RGR-d Mice

Abnormalities and degeneration of the choriocapillaris in RGR-d mice were analyzed further by immunofluorescence (Figure 7, A–C) and electron microscopy (Figure 7, E–J). Besides often thickened cytoplasm and reduction of fenestrations, many choroidal endothelial cells contained a displaced nucleus along the inner cell wall adjacent to Bruch membrane (Figures 6, F and H, and 7, H and I). Worse was endothelial atrophy, shrunken or absent lumens, or disappearance of several adjacent choroidal capillaries with replacement by extracellular material and cell nuclei (Figure 7, F and G). This complex phenotype was corroborated by immunofluorescence staining of CD31, or platelet endothelial cell adhesion molecule-1. CD31 is located on the endothelial cell surface and concentrated at intercellular junctions. The continuity and intensity of CD31 immunofluorescence staining in RGR-d mice were much lower than that in $RGR^{-/-}$ mice through a cross-section of the whole retina (Figure 7, A–C). Quantification of the CD31 immunofluorescence was significantly lower in the RGR-d mice than in $RGR^{-/-}$ mice (Figure 7D).

## Severe Retinal Degeneration in RGR-F89 Mutant Mice

Although different mutations or deletions of exon VI produced redundant exon VI–skipping RGR-d mice, the frameshift mutation in mouse line F89 generated unique mice with a truncated RGR isoform with altered carboxyl terminal amino acid sequence. At the light microscopic level, 3-month–old homozygous RGR-F89 mice showed hypertrophy within the RPE and mild changes in the retina compared with 3-month–old wild-type littermates (Figure 8, A and B). At age 23 months, RGR-F89 mice showed extraordinarily severe retinal degeneration with marked enlargement of the thickened eosinophilic band under the RPE (Figure 8, C-F). In old RGR-F89 mice, the retina from ora serrata to midperipheral area degenerated almost completely (Figure 9). Resembling RGR-d mice, RGR-F89 mice developed a continuous band of basal deposits or thickening of Bruch membrane and shared other histopathologic features during aging (Figure 10). At the ultrastructural level, large masses of granular deposits protruded from the Bruch membrane and interspersed within highly distorted basal membranes of the RPE (Figure 11).[39] The basal region of the RPE was a highly dystrophic zone of membranous material with no clear cellular boundaries. Abnormal mitochondria, distended smooth endoplasmic reticulum, dilated perinuclear space, and cytoplasmic vacuolization indicated a high level of RPE cell stress or degeneration. Large amounts of membranous debris were found in the lumen of the choriocapillaris. Although lipofuscin and melanolipofuscin granules[39] were present in the RPE of RGR-d mice at approximately 21 months of age (Figure 6, E and F), these granules were rare in the 23-month–old RGR-F89 mouse with late-stage severe photoreceptor loss.

## Evaluation of Cell Growth Inhibition for RGR and RGR-d Expressing Cell Lines

Stably transformed ARPE-19 and COS-7 cells that expressed RGR or RGR-d were analyzed to determine whether RGR-d expression affected cell growth. The cell doubling times for RGR and RGR-d cell lines were evaluated at passages 15 and 24 after transfection (Figure 12). Cells that expressed RGR-d were observed to grow significantly slower, whereas normal RGR-expressing cells proliferated at a similar rate as that of control cells (Figure 12A). The cell doubling times of ARPE-19 cell that expressed RGR-d were 30% to 37% longer than both RGR-transformed cells and vector control cells. The difference in growth rates was even greater for COS-7 cells that expressed RGR-d. The doubling times of RGR-d–transformed COS-7 were 47% to 64% longer than RGR cells and the vector control transformants. The RGR-d protein was expressed at significantly lower levels in two cell lines, ARPE-19 and LN-229, relative to the amount of normal RGR (Figure 12B).

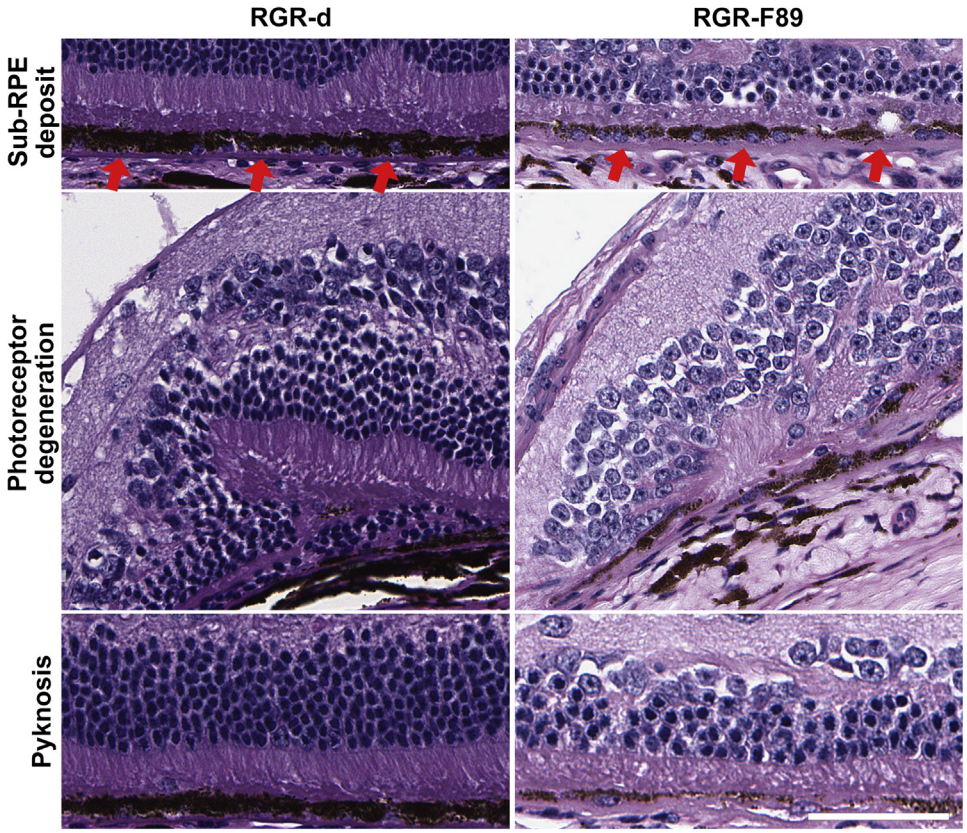


**Figure 10** Comparison of histologic features of retinal pigment epithelium (RPE) and retina from RGR-d and RGR-F89 mice. The phenotype of RGR-d and RGR-F89 mice included similar pathologic features. **Top panels:** Both RGR-d and RGR-F89 mice exhibited a continuous eosinophilic layer of sub-RPE deposits (**red arrows**). The confluent band was much thicker in RGR-F89 mice. **Middle panels:** The inner nuclear layer and outer nuclear layer (ONL) were severely disturbed, and abnormal pigments were found in the retina in both lines of mice. **Bottom panels:** Pyknosis in the ONL was significant in both RGR-d and RGR-F89 mice. In RGR-F89 mice, almost all the cells in the ONL were undergoing pyknosis with outer segment disruption and RPE degeneration. Scale bar = 50 μm.

### Mislocalization of RGR-d in Cultured Cells

The subcellular localization of RGR and RGR-d was compared in cultured cells by immunofluorescence labeling and confocal microscopy (Figure 13). ARPE-19 and LN-229 cells, that were transfected with pFLAG-hRGR, pFLAG-hRGR-d, or control pFLAG-CMV-4 expression vectors, were double labeled with anti-FLAG and calnexin-specific antibodies. The intracellular distribution of the RGR and RGR-d proteins differed significantly regardless of cell type. Normal RGR localized substantially with calnexin, an endoplasmic reticulum marker (Figure 13, A–C). In contrast to the more homogeneously distributed RGR, RGR-d coincided with conspicuous punctate speckles having a separate distribution from that of calnexin within the cytoplasm (Figure 13, D–F). The results showed that RGR, but not RGR-d, sorted mainly to the endoplasmic reticulum. Neither RGR nor RGR-d expression was observed in control cells transfected with empty pFLAG-CMV-4. Cells treated with nocodazole show rearrangement of intracellular architecture due to the disruption of microtubular polymerization.[40] Despite the effects of nocodazole, the RGR staining pattern remained in tandem with the changes in calnexin distribution (Supplemental Figure S4). In comparison, RGR-d still could be found in punctate speckles, and the lack of colocalization with the endoplasmic reticulum marker was evident (Supplemental Figure S4).

## Discussion

*RGR* gene mutations are associated with dominantly inherited, peripapillary choroidal atrophy (c.824dupG, p.I276Nfs*78), and with less certainty, autosomal recessive retinitis pigmentosa (c.196A>C, p.S66R), and other forms of retinal disease.[41–44] Although co-expressed from a normal human *RGR* gene, RGR-d is an abnormal dysfunctional protein that is associated with drusen and other histologic features of AMD patients.[32,33] It is a major isoform of human RGR opsin. The phenotype of RGR-d mice showed that the RGR-d isoform can lead to gradual ocular pathology with retinal degeneration and presents a new road toward modeling AMD in humans.

Old RGR-d mice typically develop a tall confluent band of eosinophilic material along the basal border of the RPE monolayer. RGR-d accumulates within or close to this basal region at focal concentration sites (Figure 2C). The

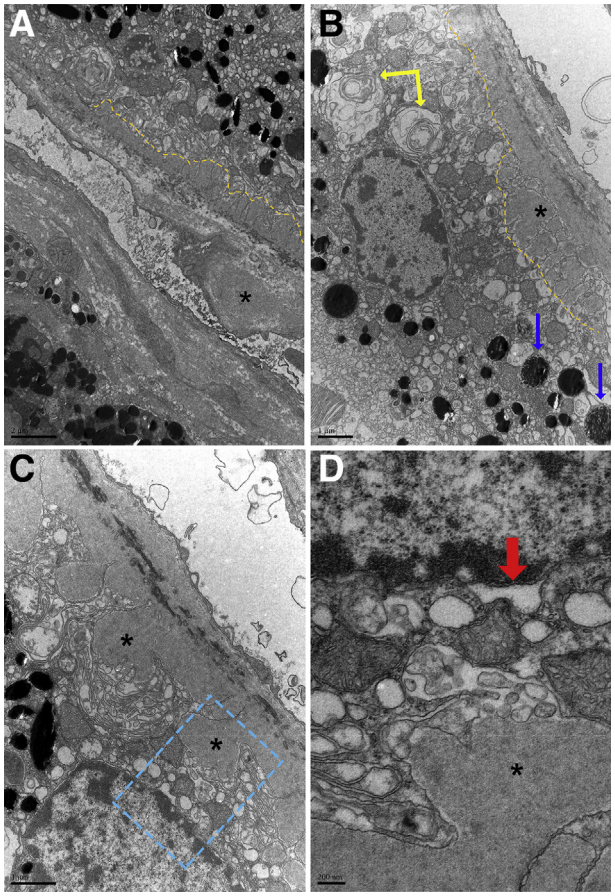


**Figure 11** Ultrastructural pathology in RGR-F89 mice. **A:** Electron microscopic analysis showed that retinal pigment epithelium (RPE) cells of homozygous RGR-F89 mice (26 months old) were highly vacuolized. Continuous granular basal deposits were seen within the Bruch membrane of varying thickness (**yellow dashed line**). Drusen-like deposits with the thickness of 2 to 4 μm were observed to project from the Bruch membrane toward the RPE and choriocapillaris (**asterisks**). **B:** In the RPE cell body, multimembranous structures with multiple vesicles wrapped inside were seen (**yellow arrow**). Some of these structures resembled multilamellar bodies. Several granules that appeared to be decaying melanosomes with splayed cords of melanoprotein (**blue arrows**) were observed at the basal side of the RPE and resembled granules that have been seen in older humans.[39] The Bruch membrane showed an undulant inner surface (**yellow dashed line**) with irregular extensions toward the RPE (**asterisks**). **C:** The basal infoldings were replaced with a highly dystrophic membranous zone that was interspersed with protrusions of granular deposits (**asterisks**) of Bruch membrane. Vesicles or membranous debris was present in the capillary lumen. **D:** The area enclosed by the **blue boxed area** in **C** is shown at higher magnification. The perinuclear space was enlarged (**red arrow**), probably indicating dilation and retention of abnormal material within the continuous smooth endoplasmic reticulum as well. Outcroppings of the Bruch membrane were characterized by a diffuse grainy deposit (**asterisk**). Scale bars: 2 μm (**A**); 1 μm (**B** and **C**); 200 nm (**D**).

accumulation of RGR-d is higher in older RGR-d mutant mice and has a histologic distribution much like that found in older humans, including sporadic targeting to the basolateral plasma membrane of some RPE cells and concentration in discrete areas next to RPE cells. In addition to the basal deposits, old RGR-d mice also developed subretinal material that distorted the ONL (Figure 4). Further study of the misaligned ONL is necessary to indicate whether these are analogues of reticular pseudodrusen or subretinal drusenoid deposits.[45,46] Müller cells also express RGR-d in these mice, as do Müller cells in humans.

The phenotypic effects of RGR-d are gradually progressive in this mouse model of AMD-like pathophysiology. All RGR-d mice developed certain pathologic features with severity dependent on old age (eg, patchy depigmentation of the fundus). Most significantly, there is significant choriocapillaris degeneration at old age and eventual retinal degeneration. At the electron microscopic level, diffuse granular-like deposits concentrated within a thickened Bruch membrane and protruded far toward the basal side of RPE. These amorphous accumulations in the Bruch membrane have been seen in other mouse models[47,48] and may reflect murine-type basal linear deposits. The basal infolding membranes of the RPE were highly disrupted, and other significant ultrastructural abnormalities were evident in the RPE cells.

In older RGR-d mice, the pathologic changes were progressively complex and not confined to the RPE and Bruch membrane as remarkably, the associated endothelial cells also degenerated with significant loss of choroidal capillaries. Because RGR-d is not expressed in the endothelial cells, the degeneration of the choriocapillaris was secondary to the RPE abnormality. A similar multifaceted interaction between the RPE and choriocapillaris may exist during normal human aging and, more so, in patients with age-related macular degeneration.[49–53] Choriocapillaris degeneration increases as humans age,[49] yet the loss of choriocapillaris density is much more advanced in AMD with notable deficit of capillaries near drusen, areas of geographic atrophy, and sites of choroidal neovascularization.[54–57] The process by which the choriocapillaris degenerates in humans or RGR-d mice is unknown. Complement-mediated injury from the deposition of membrane attack complex C5b-9 around the choriocapillaris may to lead to loss of choroidal endothelial cells, as suggested previously.[58,59] Alternatively, RGR-d expression and processing within human and mouse RPE cells may lead to cellular atrophy that impairs the trophic function of the RPE in maintenance of the choriocapillaris. In addition, RGR-d may drive the chronic release of basal deposits that are detrimental to the choroidal endothelial cells due to cytotoxicity or the burden of problematic clearance through the endothelium. Possibly, RGR-d in RPE cells also contributes to choriocapillaris degeneration in humans.

A projected consequence of the choroidal vascular defect in humans and RGR-d mice is ischemia of the RPE and retina followed by degrees of cellular atrophy and cell death.[60] The slow degeneration of the retina in these mice is consistent with the ischemia hypothesis of AMD, although other factors involving the Müller cells or RPE may play a role. The slow retinal degeneration in RGR-d mice is a more realistic model for age-related maculopathy in humans than the severe retinal degeneration seen in the RGR-F89 mice,

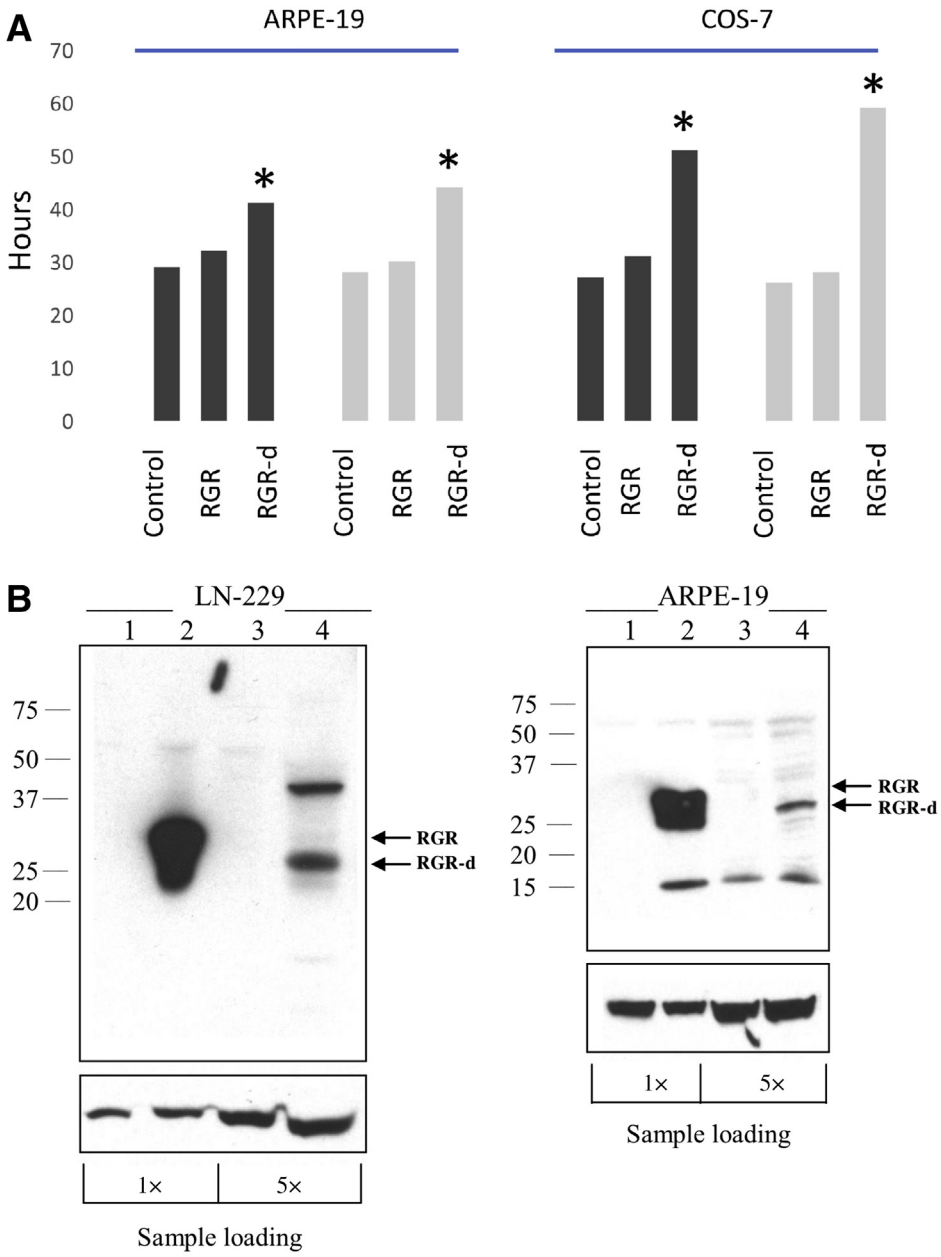


**Figure 12** Inhibition of cell growth by overexpression of RGR-d. **A:** Cell doubling times for stable cell lines that express RGR or RGR-d were compared. Cells from passage 15 and passage 24 after transfection and cell selection were analyzed. Black columns represent data collected from cells after passage 15, and gray columns represent data collected from cells after passage 24. Equal numbers of cells were inoculated into culture chamber slides with individual wells, the bottom of which were marked uniformly with three to four separate regions for subsequent visualization and counting of cells on an inverted phase contrast microscope. RGR-d cell growth was slowed markedly with cell doubling times that were 30% to 37% (ARPE-19), or 47% to 64% (COS-7), longer than that of RGR cells and vector control transformants. **B:** Western blot analysis of stably transformed LN-229 and ARPE-19 cells that express RGR or RGR-d proteins. Both cell types were transfected with pFLAG-hRGR, pFLAG-hRGR-d, or pFLAG-CMV-4 expression vectors. Whole cell extracts were analyzed. FLAG-control extracts (lanes 1 and 3), FLAG-RGR extracts (lane 2), and FLAG-RGR-d extracts (lane 4) are shown. The protein blots were probed with anti-human RGR DE7 antibody (**top blots**). Five times more whole cell FLAG-control extract and RGR-d extract was loaded into lanes 3 and 4, respectively, to increase the detection of RGR-d. The blot membranes were reprobed with anti-actin antibody to compare protein loading amounts (**bottom blots**). $^*P < 0.05$.

specially since RGR-d, and not an RGR-F89 homolog, is seen in humans. The reason for the difference in RGR-d and RGR-F89 phenotypes is unknown, although it is interesting that the pathology in RGR-F89 mice appears to overlap that in RGR-d mice. It is possible that RGR-d produces a less severe, more slowly progressing disease, because despite its abnormality, it is at least partly folded, as indicated by the ability of some RGR-d to traffic to the basolateral plasma membrane.

Neither line of mutant mice presented characteristic discrete hard drusen, although an isolated case of classic hard drusen-like basal deposit was found in a 10-

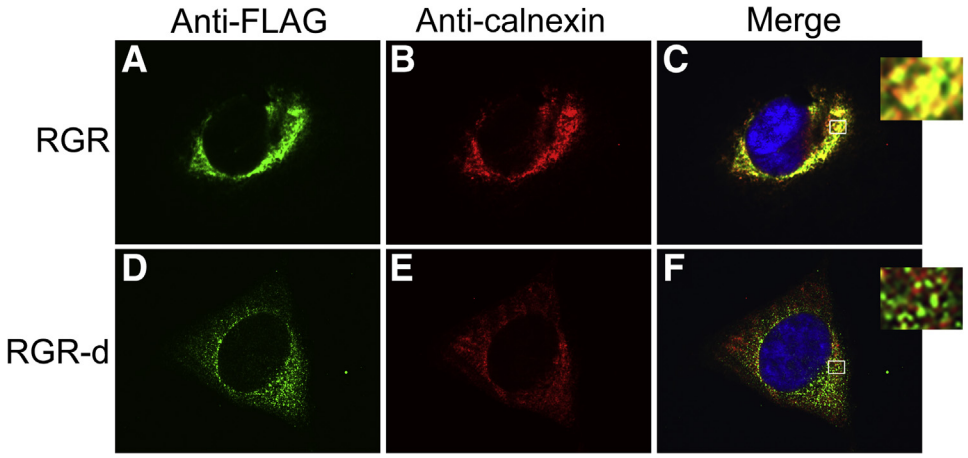


**Figure 13** Immunofluorescence localization of FLAG-RGR and FLAG-RGR-d in stably transformed LN-229 cells. **A** and **B:** Normal RGR (**A**) has a similar intracellular distribution as calnexin (**B**), an endoplasmic reticulum maker. **C:** RGR and calnexin overlap substantially, as indicated in the merged panel. The enlarged **boxed area** shows more detailed colocalization of RGR and calnexin. **D** and **E:** In contrast, the distribution of RGR-d (**D**) was distinct from that of calnexin (**E**). **F:** The **merged panel** and the enlarged **boxed area** displayed little colocalization of RGR-d with calnexin.

month−old heterozygous RGR-d (+/d) mouse (Supplemental Figure S3), indicating that such focal extracellular deposits, not reported previously, may well develop in mice. Both homozygous RGR-d and RGR-F89 mice demonstrated diffuse granular deposits in the Bruch membrane, a layer of sub-RPE material, RPE atrophy, choriocapillaris degeneration, and retinal cell loss that are relevant landmarks of age-related maculopathy in humans. The old RGR-d mice have the key features of age-related maculopathy despite having a normal environmental and genetic background in other respects. This disease model and the formation of classic hard and soft drusen in mice may be explored further by experimental disturbance of the complement system, immune status, diet, and oxidative and endoplasmic reticulum stress conditions in these mice.

There is increasing evidence that proteopathy plays a significant role in AMD and that AMD may be a protein misfolding disease.[61−63] Herein, the results indicate that mouse RGR-d protein is pathogenic and leads to several histologic features of age-related macular degeneration. Both mouse and human RGR-d accumulate *in vivo* as RPE basal deposits, as well as traffic to the basolateral plasma membrane. At a young age, human RGR-d in RPE cells localizes mainly in the basolateral plasma membrane.[32] In older humans, RGR-d is found predominantly in basal deposits in the Bruch membrane, intercapillary pillars, and most drusen, including early-stage, hard, soft, and confluent types.[33] Thus, RGR-d is widely present in human retinas, although there is variation in the amount and processing of RGR-d between young and old persons. It is possible that RGR-d protein processing or misfolding in AMD patients is pathogenic in a manner similar to that in RGR-d mutant mice. In cultured cells, the expression of RGR-d strongly inhibits cell proliferation. Such cell growth defects can be caused by the overexpression of proteins with misfolding or mislocalizing mutations.[64,65] In the LN-229 cultured cells, RGR-d is clearly mislocalized to cytoplasmic speckles, perhaps because of misfolding in this established cell line. In cultures of human fetal RPE cells, RGR-d sorts to the plasma membrane instead, and thus RGR-d is folded more appropriately in these primary cultured cells.[32] Alternate protein processing and folding of RGR-d in the different cell culture systems may reflect important protein folding behavior of RGR-d in humans during aging and disease. Henceforth, the mechanism of RGR-d proteopathy can be addressed in complementary studies of RGR-d mice and cell culture model systems.

In summary, the RGR-d mouse model validates association of certain histopathologic traits of maculopathy with the human *RGR* gene and can help analyze the mechanisms by which these traits develop. Because AMD is a complex disease with many environmental and genetic risk factors, a host of experimental conditions that strongly increase or therapeutically prevent the AMD phenotype in RGR-d mice can be studied using this novel animal model. The paradoxical notion, that a high-frequency, otherwise normal, human *RGR* gene can be pathogenic under certain conditions, will contribute to greater comprehension of the multifactorial causes of AMD.

## Acknowledgments

We thank the Transgenic/Knockout Rodent Core Facility of the University of Southern California Norris Cancer Center, Anthony Rodriguez of the USC Cell and Tissue Imaging Core, Dr. Chang Tong at the USC Stem Cell Center, and Xiaopeng Wang of the USC Translational Research In-Vivo Core Facility for valuable assistance.

## Author Contributions

X.B. designed and performed the experiments and wrote the manuscript. Z.Z. generated the CRISPR-Cas9–edited mouse lines and analyzed mouse genotype, mRNA, protein, and histology. Y.G. performed ultrastructure analysis of retinal G-protein–coupled receptor–opsin (RGR-d) mice. C.B. performed electron microscopic analysis of RGR-F89 mice and interpreted the results. H.K. performed cell culture experiments, optimized immunofluorescence, and analyzed human donor retinas. N.W. designed and performed experiments involving gene editing of mouse embryos. S.H. contributed to design of experiments and analysis of the results. X.L. and B.S. analyzed ocular pathology and interpreted the results. F.N.R.-C. performed ultrastructure analysis of mouse retina. A.A.S. contributed to analysis and evaluation of the results. L.H. performed ultrastructure analysis of RGR-d mice. M.Z. planned and supervised the project and analyzed and interpreted the data. H.K.W.F. designed and directed the experiments and wrote the manuscript with participation from all authors.

## Supplemental Data

Supplemental material for this article can be found at *http://doi.org/10.1016/j.ajpath.2021.05.003*.

## References


1. Irvine GB, El-Agnaf OM, Shankar GM, Walsh DM: Protein aggregation in the brain: the molecular basis for Alzheimer's and Parkinson's diseases. Mol Med 2008, 14:451–464
2. Sweeney P, Park H, Baumann M, Dunlop J, Frydman J, Kopito R, McCampbell A, Leblanc G, Venkateswaran A, Nurmi A, Hodgson R: Protein misfolding in neurodegenerative diseases: implications and strategies. Transl Neurodegener 2017, 6:6
3. Chirco KR, Sohn EH, Stone EM, Tucker BA, Mullins RF: Structural and molecular changes in the aging choroid: implications for age-related macular degeneration. Eye (Lond) 2017, 31:10–25
4. Sarks S, Sarks J: Age-related maculopathy: nonneovascular age-related macular degeneration and the evolution of geographic atrophy. Edited by Ryan SJ. In Retina. ed 3. Philadelphia, PA: Mosby Inc., 2001
5. Lengyel I, Tufail A, Hosaini HA, Luthert P, Bird AC, Jeffery G: Association of drusen deposition with choroidal intercapillary pillars in the aging human eye. Invest Ophthalmol Vis Sci 2004, 45: 2886–2892
6. Rudolf M, Clark ME, Chimento MF, Li CM, Medeiros NE, Curcio CA: Prevalence and morphology of druse types in the macula and periphery of eyes with age-related maculopathy. Invest Ophthalmol Vis Sci 2008, 49:1200–1209
7. Curcio CA: Antecedents of soft drusen, the specific deposits of age-related macular degeneration, in the biology of human macula. Invest Ophthalmol Vis Sci 2018, 59:AMD182–AMD194
8. Fritsche LG, Igl W, Bailey JN, Grassmann F, Sengupta S, Bragg-Gresham JL, et al: A large genome-wide association study of age-related macular degeneration highlights contributions of rare and common variants. Nat Genet 2016, 48:134–143
9. Ratnapriya R, Sosina OA, Starostik MR, Kwicklis M, Kapphahn RJ, Fritsche LG, Walton A, Arvanitis M, Gieser L, Pietraszkiewicz A, Montezuma SR, Chew EY, Battle A, Abecasis GR, Ferrington DA, Chatterjee N, Swaroop A: Retinal transcriptome and eQTL analyses identify genes associated with age-related macular degeneration. Nat Genet 2019, 51:606–610
10. Wang L, Clark ME, Crossman DK, Kojima K, Messinger JD, Mobley JA, Curcio CA: Abundant lipid and protein components of drusen. PLoS One 2010, 5:e10329
11. Crabb JW: The proteomics of drusen. Cold Spring Harb Perspect Med 2014, 4:a017194
12. Johnson LV, Forest DL, Banna CD, Radeke CM, Maloney MA, Hu J, Spencer CN, Walker AM, Tsie MS, Bok D, Radeke MJ, Anderson DH: Cell culture model that mimics drusen formation and triggers complement activation associated with age-related macular degeneration. Proc Natl Acad Sci U S A 2011, 108:18277–18282
13. Galloway CA, Dalvi S, Hung SSC, MacDonald LA, Latchney LR, Wong RCB, Guymer RH, Mackey DA, Williams DS, Chung MM, Gamm DM, Pebay A, Hewitt AW, Singh R: Drusen in patient-derived hiPSC-RPE models of macular dystrophies. Proc Natl Acad Sci U S A 2017, 114:E8214–E8223
14. Usui H, Nishiwaki A, Landiev L, Kacza J, Eichler W, Wako R, Kato A, Takase N, Kuwayama S, Ohashi K, Yafai Y, Bringmann A, Kubota A, Ogura Y, Seeger J, Wiedemann P, Yasukawa T: In vitro drusen model - three-dimensional spheroid culture of retinal pigment epithelial cells. J Cell Sci 2018, 132:jcs215798
15. Crabb JW, Miyagi M, Gu X, Shadrach K, West KA, Sakaguchi H, Kamei M, Hasan A, Yan L, Rayborn ME, Salomon RG, Hollyfield JG: Drusen proteome analysis: an approach to the etiology of age-related macular degeneration. Proc Natl Acad Sci U S A 2002, 99:14682–14687
16. Curcio CA: Soft drusen in age-related macular degeneration: biology and targeting via the oil spill strategies. Invest Ophthalmol Vis Sci 2018, 59:AMD160–AMD181
17. Notomi S, Ishihara K, Efstathiou NE, Lee JJ, Hisatomi T, Tachibana T, Konstantinou EK, Ueta T, Murakami Y, Maidana DE, Ikeda Y, Kume S, Terasaki H, Sonoda S, Blanz J, Young L, Sakamoto T, Sonoda KH, Saftig P, Ishibashi T, Miller JW, Kroemer G, Vavvas DG: Genetic LAMP2 deficiency accelerates the age-associated formation of basal laminar deposits in the retina. Proc Natl Acad Sci U S A 2019, 116:23724–23734
18. Jiang M, Pandey S, Fong HK: An opsin homologue in the retina and pigment epithelium. Invest Ophthalmol Vis Sci 1993, 34: 3669–3678
19. Jiang M, Shen D, Tao L, Pandey S, Heller K, Fong HK: Alternative splicing in human retinal mRNA transcripts of an opsin-related protein. Exp Eye Res 1995, 60:401–406
20. Fong HK, Lin MY, Pandey S: Exon-skipping variant of RGR opsin in human retina and pigment epithelium. Exp Eye Res 2006, 83: 133–140
21. Shen D, Jiang M, Hao W, Tao L, Salazar M, Fong HK: A human opsin-related gene that encodes a retinaldehyde-binding protein. Biochemistry 1994, 33:13117–13125
22. Zhang Z, Fong HKW: Coexpression of nonvisual opsin, retinal G protein-coupled receptor, and visual pigments in human and bovine cone photoreceptors. Mol Vis 2018, 24:434–442
23. Hao W, Fong HK: Blue and ultraviolet light-absorbing opsin from the retinal pigment epithelium. Biochemistry 1996, 35:6251–6256
24. Hao W, Fong HK: The endogenous chromophore of retinal G protein-coupled receptor opsin from the pigment epithelium. J Biol Chem 1999, 274:6085–6090
25. Chen P, Hao W, Rife L, Wang XP, Shen D, Chen J, Ogden T, Van Boemel GB, Wu L, Yang M, Fong HK: A photic visual cycle of rhodopsin regeneration is dependent on Rgr. Nat Genet 2001, 28: 256–260
26. Maeda T, Van Hooser JP, Driessen CA, Filipek S, Janssen JJ, Palczewski K: Evaluation of the role of the retinal G protein-coupled receptor (RGR) in the vertebrate retina in vivo. J Neurochem 2003, 85:944–956

27. Wenzel A, Oberhauser V, Pugh EN, Lamb TD, Grimm C, Samardzija M, Fahl E, Seeliger MW, Remé CE, von Lintig J: The retinal G protein-coupled receptor (RGR) enhances isomerohydrolase activity independent of light. J Biol Chem 2005, 280: 29874–29884
28. Radu RA, Hu J, Peng J, Bok D, Mata NL, Travis GH: Retinal pigment epithelium-retinal G protein receptor-opsin mediates light-dependent translocation of all-trans-retinyl esters for synthesis of visual chromophore in retinal pigment epithelial cells. J Biol Chem 2008, 283:19730–19738
29. Morshedian A, Kaylor JJ, Ng SY, Tsan A, Frederiksen R, Xu T, Yuan L, Sampath AP, Radu RA, Fain GL, Travis GH: Light-driven regeneration of cone visual pigments through a mechanism involving RGR opsin in Muller glial cells. Neuron 2019, 102: 1172–1183.e5
30. Choi EH, Daruwalla A, Suh S, Leinonen H, Palczewski K: Retinoids in the visual cycle: role of the retinal G protein-coupled receptor. J Lipid Res 2021, 62:100040
31. Lin MY, Kochounian H, Moore RE, Lee TD, Rao N, Fong HK: Deposition of exon-skipping splice isoform of human retinal G protein-coupled receptor from retinal pigment epithelium into Bruch's membrane. Mol Vis 2007, 13:1203–1214
32. Kochounian H, Zhang Z, Spee C, Hinton DR, Fong HK: Targeting of exon VI-skipping human RGR-opsin to the plasma membrane of pigment epithelium and co-localization with terminal complement complex C5b-9. Mol Vis 2016, 22:213–223
33. Kochounian H, Johnson LV, Fong HK: Accumulation of extracellular RGR-d in Bruch's membrane and close association with drusen at intercapillary regions. Exp Eye Res 2009, 88:1129–1136
34. Pennesi ME, Neuringer M, Courtney RJ: Animal models of age related macular degeneration. Mol Aspects Med 2012, 33: 487–509
35. Forest DL, Johnson LV, Clegg DO: Cellular models and therapies for age-related macular degeneration. Dis Model Mech 2015, 8:421–427
36. Marmorstein LY, McLaughlin PJ, Peachey NS, Sasaki T, Marmorstein AD: Formation and progression of sub-retinal pigment epithelium deposits in Efemp1 mutation knock-in mice: a model for the early pathogenic course of macular degeneration. Hum Mol Genet 2007, 16:2423–2432
37. Tao L, Shen D, Pandey S, Hao W, Rich KA, Fong HK: Structure and developmental expression of the mouse RGR opsin gene. Mol Vis 1998, 4:25
38. Handala L, Fiore T, Rouille Y, Helle F: QuantIF: an ImageJ macro to automatically determine the percentage of infected cells after immunofluorescence. Viruses 2019, 11:165
39. Feeney L: Lipofuscin and melanin of human retinal pigment epithelium: fluorescence, enzyme cytochemical, and ultrastructural studies. Invest Ophthalmol Vis Sci 1978, 17:583–600
40. Vasquez RJ, Howell B, Yvon AM, Wadsworth P, Cassimeris L: Nanomolar concentrations of nocodazole alter microtubule dynamic instability in vivo and in vitro. Mol Biol Cell 1997, 8:973–985
41. Morimura H, Saindelle-Ribeaudeau F, Berson EL, Dryja TP: Mutations in RGR, encoding a light-sensitive opsin homologue, in patients with retinitis pigmentosa. Nat Genet 1999, 23:393–394
42. Arno G, Hull S, Carss K, Dev-Borman A, Chakarova C, Bujakowska K, van den Born LI, Robson AG, Holder GE, Michaelides M, Cremers FP, Pierce E, Raymond FL, Moore AT, Webster AR: Reevaluation of the retinal dystrophy due to recessive alleles of RGR with the discovery of a cis-acting mutation in CDHR1. Invest Ophthalmol Vis Sci 2016, 57:4806–4813
43. Li J, Xiao X, Li S, Jia X, Guo X, Zhang Q: RGR variants in different forms of retinal diseases: the undetermined role of truncation mutations. Mol Med Rep 2016, 14:4811–4815
44. Ba-Abbad R, Leys M, Wang X, Chakarova C, Waseem N, Carss KJ, Raymond FL, Bujakowska KM, Pierce EA, Mahroo OA, Mohamed MD, Holder GE, Hummel M, Arno G, Webster AR: Clinical features of a retinopathy associated with a dominant allele of the RGR gene. Invest Ophthalmol Vis Sci 2018, 59:4812–4820
45. Wightman AJ, Guymer RH: Reticular pseudodrusen: current understanding. Clin Exp Optom 2019, 102:455–462
46. Chen L, Messinger JD, Zhang Y, Spaide RF, Freund KB, Curcio CA: Subretinal drusenoid deposit in age-related macular degeneration: histologic insights into initiation, progression to atrophy, and imaging. Retina 2020, 40:618–631
47. Song D, Mohammed I, Bhuyan R, Miwa T, Williams AL, Gullipalli D, Sato S, Song Y, Dunaief JL, Song WC: Retinal basal laminar deposits in complement fH/fP mouse model of dense deposit disease. Invest Ophthalmol Vis Sci 2018, 59:3405–3415
48. Malek G, Busik J, Grant MB, Choudhary M: Models of retinal diseases and their applicability in drug discovery. Expert Opin Drug Discov 2018, 13:359–377
49. Ramrattan RS, van der Schaft TL, Mooy CM, de Bruijn WC, Mulder PG, de Jong PT: Morphometric analysis of Bruch's membrane, the choriocapillaris, and the choroid in aging. Invest Ophthalmol Vis Sci 1994, 35:2857–2864
50. Bhutto I, Lutty G: Understanding age-related macular degeneration (AMD): relationships between the photoreceptor/retinal pigment epithelium/Bruch's membrane/choriocapillaris complex. Mol Aspects Med 2012, 33:295–317
51. Biesemeier A, Taubitz T, Julien S, Yoeruek E, Schraermeyer U: Choriocapillaris breakdown precedes retinal degeneration in age-related macular degeneration. Neurobiol Aging 2014, 35: 2562–2573
52. Campos MM, Abu-Asab MS: Loss of endothelial planar cell polarity and cellular clearance mechanisms in age-related macular degeneration. Ultrastruct Pathol 2017, 41:312–319
53. Sohn EH, Flamme-Wiese MJ, Whitmore SS, Workalemahu G, Marneros AG, Boese EA, Kwon YH, Wang K, Abramoff MD, Tucker BA, Stone EM, Mullins RF: Choriocapillaris degeneration in geographic atrophy. Am J Pathol 2019, 189:1473–1480
54. McLeod DS, Grebe R, Bhutto I, Merges C, Baba T, Lutty GA: Relationship between RPE and choriocapillaris in age-related macular degeneration. Invest Ophthalmol Vis Sci 2009, 50: 4982–4991
55. Mullins RF, Johnson MN, Faidley EA, Skeie JM, Huang J: Choriocapillaris vascular dropout related to density of drusen in human eyes with early age-related macular degeneration. Invest Ophthalmol Vis Sci 2011, 52:1606–1612
56. Seddon JM, McLeod DS, Bhutto IA, Villalonga MB, Silver RE, Wenick AS, Edwards MM, Lutty GA: Histopathological insights into choroidal vascular loss in clinically documented cases of age-related macular degeneration. JAMA Ophthalmol 2016, 134: 1272–1280
57. Dryja TP: Early insight into neovascular age-related macular degeneration. JAMA Ophthalmol 2016, 134:1281–1282
58. Mullins RF, Schoo DP, Sohn EH, Flamme-Wiese MJ, Workamelahu G, Johnston RM, Wang K, Tucker BA, Stone EM: The membrane attack complex in aging human choriocapillaris: relationship to macular degeneration and choroidal thinning. Am J Pathol 2014, 184:3142–3153
59. Chirco KR, Tucker BA, Stone EM, Mullins RF: Selective accumulation of the complement membrane attack complex in aging choriocapillaris. Exp Eye Res 2016, 146:393–397
60. Feigl B: Age-related maculopathy - linking aetiology and pathophysiological changes to the ischaemia hypothesis. Prog Retin Eye Res 2009, 28:63–86
61. Ferrington DA, Sinha D, Kaarniranta K: Defects in retinal pigment epithelial cell proteolysis and the pathology associated with age-related macular degeneration. Prog Retin Eye Res 2016, 51:69–89
62. Golestaneh N, Chu Y, Xiao YY, Stoleru GL, Theos AC: Dysfunctional autophagy in RPE, a contributing factor in age-related macular degeneration. Cell Death Dis 2017, 8:e2537

63. Blasiak J, Pawlowska E, Szczepanska J, Kaarniranta K: Interplay between autophagy and the ubiquitin-proteasome system and its role in the pathogenesis of age-related macular degeneration. Int J Mol Sci 2019, 20:210
64. Geiler-Samerotte KA, Dion MF, Budnik BA, Wang SM, Hartl DL, Drummond DA: Misfolded proteins impose a dosage-dependent fitness cost and trigger a cytosolic unfolded protein response in yeast. Proc Natl Acad Sci U S A 2011, 108:680–685
65. Kintaka R, Makanae K, Moriya H: Cellular growth defects triggered by an overload of protein localization processes. Sci Rep 2016, 6: 31774